NOTICE

The quality of this microfiche is heavily dependent upon the quality of the original thesis submitted for microfilming. Every effort has been made to ensure the highest quality of reproduction possible.

If pages are missing, contact the university which granted the degree.

Some pages may have indistinct print especially if the original pages were typed with a poor typewriter ribbon or if the university sent us a poor photocopy.

Previously copyrighted materials (journal articles, published tests, etc.) are not filmed.

Reproduction in full or in part of this film is governed by the Canadian Copyright Act, R.S.C. 1970, c. C-30. Please read the authorization forms which accompany this thesis.

THIS DISSERTATION
HAS BEEN MICROFILMED
EXACTLY AS RECEIVED

AVIS

La qualité de cette microfiche dépend grandement de la qualité de la thèse soumise au microfilmage. Nous avons tout fait pour assurer une qualité supérieure de reproduction.

S'il manque des pages, veuillez communiquer avec l'université qui a conféré le grade.

La qualité d'impression de certaines pages peut laisser à désirer, surtout si les pages originales ont été dactylographiées à l'aide d'un ruban usé ou si l'université nous a fait parvenir une photocopie de mauvaise qualité.

Les documents qui font déjà l'objet d'un droit d'auteur (articles de revue, examens publiés, etc.) ne sont pas microfilmés.

La reproduction, même partielle, de ce microfilm est soumise à la Loi canadienne sur le droit d'auteur, SRC 1970, c. C-30. Veuillez prendre connaissance des formules d'autorisation qui accompagnent cette thèse.

LA THÈSE A ÉTÉ
MICROFILMÉE TELLE QUE
NOUS L'AVONS REÇUE

UNIVERSITÉ D'OTTAWA
UNIVERSITY OF OTTAWA

A CONTRIBUTION TO THEORETICAL AND EXPERIMENTAL CHARACTERIZATION OF MICROSTRIP DISCONTINUITIES

by

Asoknath Chattopadhyay

Submitted to the School of Graduate Studies
in partial fulfilment of the requirements
for the degree of Doctor of Philosophy

Department of Electrical Engineering
Faculty of Science and Engineering
University of Ottawa
Ottawa, Canada
February, 1976

ABSTRACT

In microwave integrated circuit design, the electrical parameters of all discontinuities must be predicted. In this thesis, theoretical and experimental characterization of some microstrip discontinuities are studied and discussed. For the theoretical approach, an approximate Green's function is derived using Wheeler's parallel plate model. In terms of this Green's function and approximate source functions, the equivalent T-circuit parameters of a general discontinuity are derived from a variational expression. In the experimental part, a comprehensive general analysis, the measurement technique and experimental arrangement for a microstrip ring containing a reciprocal discontinuity is given. For example, the parameters of thin transverse metallic plates and circular cylindrical metallic posts are measured in the quasi-TEM range and compared to theoretical values. Good overall agreement is obtained. It is believed that the resonant ring method described in this thesis is the most accurate method available to date for experimental characterization of microstrip discontinuities.

ACKNOWLEDGEMENTS

The author wishes to express his gratitude and sincere thanks to Dr. W. J. R. Hoefer for his invaluable help and guidance throughout the entire period of this work.

Thanks are due to Mr. H. A. Sayeed for his help in preparing some of the illustrations for the manuscript and to Mme. Lucie LeBlanc for the typing assistance.

Special word of thanks to my parents, my wife Kajal and my brother Amit for their unfailing encouragement.

The Communications Research Centre, Ottawa fabricated and supplied the microstrip rings used during the course of experimental investigations. This help is gratefully acknowledged.

The financial support provided by the Province of Ontario and the National Research Council of Canada through graduate Fellowships is gratefully acknowledged.

TABLE OF CONTENTS

CHAPTER 1

Introduction

In the design of any microwave circuit, particularly in integrated circuit design, the electrical parameters of all discontinuities must be predicted. Theoretical or empirical expressions relating such parameters with the geometry and properties of the structure in question are required. At the same time sufficiently accurate measurement methods should be available for the two following purposes - to verify the theoretically predicted performance and to determine the parameters when theoretical approaches are not practical due to complexity of the discontinuity.

In this thesis, both aspects, namely theoretical determination and experimental characterization of some microstrip discontinuities are studied and discussed.

Many authors [1-7] have solved theoretically the problem of discontinuity parameters in microstrip lines under static approximations. Dynamic solutions for such problems are difficult since exact expressions are available neither for the higher order modes nor for a dynamic Green's function in open microstrip structures.

The main difficulty in measuring the circuit parameters of microstrip discontinuities resides in the elimination of systematic errors introduced by coaxial-to-microstrip transitions. This problem can be avoided by testing the discontinuities in a microstrip ring [10, 11, 12, 23]. A generalized theory of the resonant ring with a wide variety of discontinuities is also presented in this thesis.

For the theoretical approach discussed in this thesis, an approximate dynamic Green's function is derived using Wheeler's [8] parallel plate model with magnetic sidewalls. The general discontinuity has been represented by an equivalent T-circuit. With the help of a variational

expression [21], the parameters of the equivalent circuit can be obtained in terms of the Green's function and approximate current distribution functions over the obstacle's surface. For example, specific expressions for the parameters of thin transverse metallic plates and circular cylindrical metallic posts are given.

For the experimental approach, a comprehensive general analysis of a microstrip ring containing a reciprocal discontinuity is given. The measurement technique and an experimental arrangement are described. Actual measurements were made on thin transverse metallic plates and circular cylindrical metallic posts to compare with the results obtained theoretically. Finally an analysis of the errors involved in resonant ring measurements is presented.

CHAPTER 2

The Microstrip Model

The exact solution of the inhomogeneous wave equation governing the field distribution in the presence of a discontinuity is rather cumbersome in a microstrip transmission line. It is therefore attempted to solve the problem using a parallel plate equivalent derived by Wheeler [8].

In an actual microstrip transmission line structure, as shown in Figure 2.1a, the energy is not confined to the width of the strip, i.e w. A fringing effect occurs, and the energy is contained in all the space around the strip width. Wheeler has given an ideal parallel plate model for the microstrip with magnetic sidewalls, as shown in Figure 2.1b. The basic idea behind the model is that the energy in a microstrip, instead of flowing in all the space around the stripwidth w, is contained in a homogeneous state over a larger cross-section A.

This parallel plate model describes very accurately the propagation of the TEM-mode in a microstrip transmission line. It can be expected that the higher modes in this model describe at least approximately the higher modes in the original structure, particularly in the vicinity of the centre of the cross-section where the propagating fields are nearly homogeneous.

Figures 2.1a and 2.1b clearly show the relationship between the parameters of the actual microstrip transmission line and those of the model. For the model, Green's functions and mode expressions can be derived in closed form, thanks to the well defined boundary conditions.

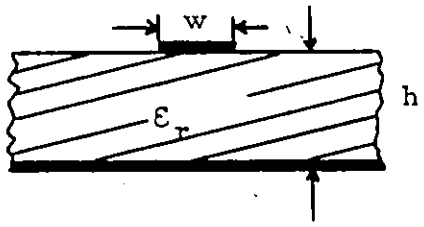

Figure 2.1 a Cross-section of a microstrip line.

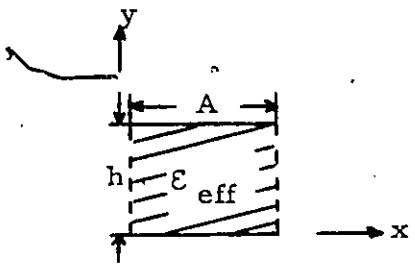

$$\varepsilon_{eff} = \left(\frac{\lambda_0}{\lambda_t}\right)^2$$

= effective dielectric constant

$$A = \frac{h}{Z_0}\sqrt{\frac{\mu_0}{\varepsilon_0 \varepsilon_{eff}}}$$

where Z_0 is the characteristic impedance of the line.

Figure 2.1 b Equivalent parallel plate model.

CHAPTER 3

Analysis of the Scattering Problem

The effect of a discontinuity upon the lowest mode in the microstrip line can be represented by an equivalent circuit. It can be shown that [21] a general discontinuity can be represented by a conventional T-section. As an example, Figure 3.1 shows a transverse obstacle in the microstrip model and its equivalent lumped element circuit in the z = 0 plane, where we indicate also the adopted conventions with regard to the positive sense of current and voltage.

We note that in general three parameters, namely, Z_{11}, Z_{12} and Z_{22} are required to describe in complete detail the effect of an obstacle on the propagating mode. However when the obstacle is symmetrical and the reference plane is symmetrically located with respect to it, the number of parameters is reduced to two, since by symmetry Z_{11} must equal Z_{22}. Furthermore, in view of this symmetry, we can represent the electric field by a sum of even and odd functions about the z = 0 plane [21]. In the even case, the obstacle is excited by waves of equal phase and amplitude which are incident from both sides. In the odd case, these two waves are in phase opposition. In terms of Figure 3.1, $V_1 = V_2 = V_e$ for even excitation. We must also have $I_1 = I_2 = I_e$ in view of the definition of the positive sense of current flow. This case corresponds to the presence of a magnetic wall at z = 0, upon which the tangential magnetic field vanishes and the electric field is a maximum. For the odd excitation, by completely analogous arguments, $V_1 = -V_2 = V_o$ and $I_1 = -I_2 = I_o$. Such a situation corresponds to a metallic wall closing off the line in the z = 0 plane. So, for symmetrical obstacles, the input impedances in the even and odd cases can be given respectively by $Z_{11} + Z_{12} = V_e/I_e$ and $Z_{11} - Z_{12} = V_o/I_o$. In Fig. 3.2, the bisected equivalent circuit of a symmetrical (about z =o plane) obstacle and the half circuits for even and odd mode excitations

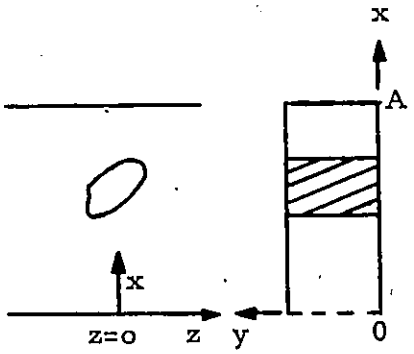

Transverse obstacle in the microstrip model.

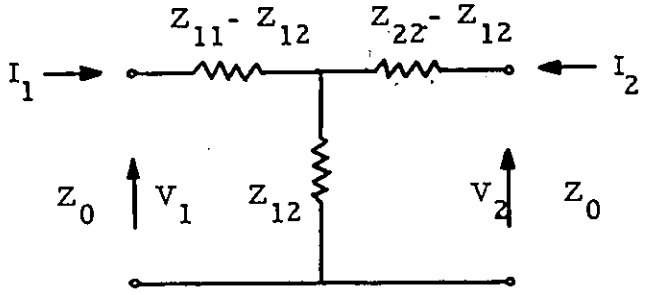

Equivalent lumped circuit in the z=o plane.

Figure 3.1

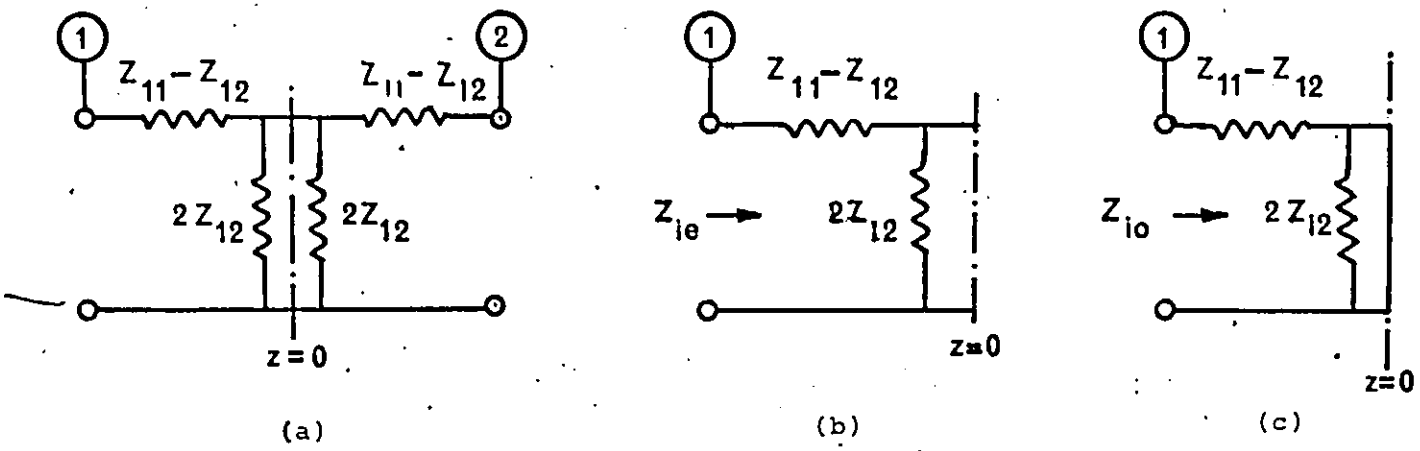

Figure 3.2 (a) Equivalent circuit of a symmetrical discontinuity.
(b) One half of the equivalent circuit for even excitation $Z_{ie} = Z_{11}+Z_{12}$.
(c) One half of the equivalent circuit for odd excitation $Z_{io} = Z_{11}-Z_{12}$.

are shown. By calculating the input impedance of the structure in the case of even and odd excitation, the equivalent parameters of the discontinuity can be computed.

In the following the even and odd impedances are calculated using variational expressions containing a Green's function and a current distribution function with respect to which the impedance expressions are stationary. In the whole process, it is assumed that only the TEM-mode can propagate in the model, all higher order modes are cutoff. The waveguide is matched at both ends.

3.1 Statement of the problem

Since the electric field vector of the incident wave is independent of y and the post is also cylindrically symmetric about the y-axis, the total field in the waveguide has only a y-component

$$\overline{E}(x,y,z) = E(x,z)\overline{u}_y \qquad (3.1.1)$$

We can thus consider $E(x,z)$ as a scalar quantity depending only on the variables x and z. The general solution of the problem must therefore obey the two dimensional scalar wave equation

$$\phi(x,z) = \phi^{inc}(x,z) + \int_{\text{obstacle}} G(x,z;\, x',\, z')\, K(x',z')\, dS' \qquad (3.1.2)$$

where $\phi^{inc}(x,z)$ represents the incident field (homogeneous TEM-solution) and the integral is the particular solution, i.e. the field produced by the currents on the surface of the cylinder. $G(x,z;\, x',\, z')$ is the Green's function, which we shall define as follows : $jkc\mu G(x,z;\, x',\, z')$ is the electric field produced at the point (x,z) by a unit current filament in the y-direction at the point $(x',\, z')$.

$K(x',z')$ is $jkc\mu J$, when J is the surface current density on the obstacle (which is in the y-direction only) and k is the propagation constant.

$\phi(x,z)$ is subject to the following boundary conditions :

i) $\frac{\partial \phi}{\partial x} = 0$ on the magnetic sidewalls at $x = 0$ and $x = A$

ii) $\phi = 0$ on the obstacle surface.

The variational expressions for the even and odd impedances are then as follows [21]:

$$Z_{11} + Z_{12} = j2kA \frac{\iint_{\text{obstacle}} K_e(x,z)\, G'(x,z;\, x',\, z')\, K_e(x',\, z')\, dS dS'}{\left[\int_{\text{obstacle}} K_e(x,z)\, \psi_e(x,z)\, dS\right]^2} \qquad (3.1.3)$$

$$\frac{1}{Z_{11} - Z_{12}} = j2kA \frac{\iint_{\text{obstacle}} K_o(x,z)\, G'(x,z;\, x',z')\, K_o(x',z')\, dS\, dS'}{\left[\int_{\text{obstacle}} K_o(x,z)\, \psi_o(x,z)\, dS\right]^2} \qquad (3.1.4)$$

In these expressions, G' is the real part of the Green's function defined earlier. K_e and K_o are the even and odd current distribution functions on the cylinder, and ψ_e and ψ_o are the even and odd standing wave fields of the fundamental mode. $k = \frac{2\pi}{\lambda_t}$, where λ_t is the wavelength of the TEM - mode on the line.

3.2 Evaluation of The Green's Function $G(x,z;\, x',\, z')$

From its definition, the Green's function must satisfy the inhomogeneous wave equation

$$\left(\frac{\partial^2}{\partial x^2} + \frac{\partial^2}{\partial z^2} + k^2\right) G(x,z\,;\, x',z') = +\,\delta(x-x')\,\delta(z-z') \qquad (3.2.1)$$

where $k = 2\pi/\lambda_t$ = propagation constant of quasi-TEM mode.

The boundary conditions on G are :

(A) $\frac{\partial G}{\partial x} = 0$ on the magnetic sidewalls at $x = 0$, A since it is an electric field in y - direction

(B) G must represent outgoing waves from the point x', z' since the current filaments on the obstacle act like sources, not like sinks.

In view of condition (A), we can express the x-dependence of G in terms of a set of cosine functions in x. Thus,

$$G = \sum_{m=o}^{\infty} \cos \frac{m\pi x}{A} \cos \frac{m\pi x'}{A} f_m(z, z', x') \qquad (3.2.2)$$

where the index $m = 0$ represents the TEM-mode in the mode spectrum of the microstrip model. Substituting this equation into (3.2.1), we have

$$\sum_{m=o}^{\infty} \left(\frac{\partial^2}{\partial z^2} + k_m^2 \right) \cos \frac{m\pi x}{A} \cos \frac{m\pi x'}{A} f_m(z, z', x') = \delta(x-x') \; \delta(z-z') \qquad (3.2.3)$$

where $k_m^2 = k^2 - \left(\frac{m\pi}{A}\right)^2$; $k_{m=o} = k$ (3.2.4)

Using the orthogonal properties of the cos-functions, the individual terms of this sum can be isolated, yielding one differential equation for each m. The right and left hand sides of (3.2.3) are multiplied by $\cos \frac{m\pi x}{A}$ and then integrated with respect to x from $x = 0$ to $x = A$.

For $m = 0$, $\cos \frac{m\pi x}{A} = 1$, and we have,

$$\int_{x=o}^{A} \sum_{m=o}^{\infty} \left(\frac{\partial^2}{\partial z^2} + k_m^2 \right) \cos \frac{m\pi x}{A} \cdot 1 \cdot \cos \frac{m\pi x'}{A} f_m(z, z', x') \, dx = \int_{x=o}^{A} 1 \; \delta(x-x') \; \delta(z-z') dx \qquad (3.2.5)$$

Except for the term with $m = o$, the integral on the left hand side is zero, and we obtained a differential equation for the function $f_o(z, z', x')$ as follows:

$$\left(\frac{\partial^2}{\partial z^2} + k^2 \right) \cdot 1 \cdot f_o(z, z', x') = \frac{1}{A} \; \delta(z-z') \qquad (m=o) \qquad (3.2.6)$$

For all higher terms $m > o$, we obtain :

$$\int_{x=o}^{A} \cos\frac{m\pi x}{A} \sum_{m=o}^{\infty} \left(\frac{\partial^2}{\partial z^2} + k_m^2\right)\cos\frac{m\pi x}{A}\cos\frac{m\pi x'}{A} f_m(z,z',x')\,dx = \int_{x=o}^{A}\cos\frac{m\pi x}{A}\,\delta(x-x')\,\delta(z-z')dx \tag{3.2.7}$$

which yields a differential equation for f_m as follows :

$$\left(\frac{\partial^2}{\partial z^2} + k_m^2\right) f_m(z,z',x') = \frac{2}{A}\,\delta(z-z') \qquad (m > 0) \tag{3.2.8}$$

For $z \neq z'$, f_o as well as f_m satisfy the homogeneous wave equation, and since they represent, according to condition (B), outgoing waves from x', z', we obtain :

$$\begin{aligned} f_m &= C_m e^{jk_m(z-z')} && \text{for } z < z' \\ \text{and}\quad f_m &= C_m e^{-jk_m(z-z')} && \text{for } z > z' \end{aligned} \tag{3.2.9}$$

This expression is correct for all m, including m = 0. We have supposed a $e^{j\omega t}$ time dependence.

C_m is the same for both cases since G must be continuous across $z = z'$ plane. In order to determine C_m, we integrate the left hand side of equation (3.2.8) once with respect to z.

We have

$$\int_{z=z'-o}^{z=z'+o} \left(\frac{\partial^2}{\partial z^2} + k_m^2\right) f_m dz = \frac{\partial f_m}{\partial z}\Big|_{z'-o}^{z'+o} + k_m^2 f_m\,[(z'+o) - (z'-o)] \tag{3.2.10}$$

The second term on the right hand side must vanish because f_m is continuous through the $z = z'$ plane. Thus

$$\frac{\partial f_o}{\partial z}\Big|_{z'-o}^{z'+o} = \frac{1}{A}\int_{z'-o}^{z'+o}\delta(z-z')\,dz = \frac{1}{A} \qquad (m = o) \tag{3.2.11}$$

and

$$\frac{\partial f_m}{\partial z}\Big|_{z'-o}^{z'+o} = \frac{2}{A}\int_{z'-o}^{z'+o}\delta(z-z')dz = \frac{2}{A} \qquad (m > o) \tag{3.2.12}$$

On the other hand, it is clearly seen from equation (3.2.9) that

$$\frac{\partial f_m}{\partial z}\Big|_{z'+o} = -jk_m C_m \quad ; \quad \frac{\partial f_m}{\partial z}\Big|_{z'-o} = jk_m C_m \quad \text{(all m)} \quad (3.2.13)$$

Therefore

$$\frac{\partial f_m}{\partial z}\Big|_{z'-o}^{z'+o} = -j2k_m C_m \quad (3.2.14)$$

And we obtain expressions for C_m by combining (3.2.14) with (3.2.11) and (3.2.12).

$$C_o = -\frac{j}{2kA} \quad \text{(for } m=o\text{)} \quad (3.2.15)$$

and $$C_m = \frac{j}{k_m A} \quad \text{(for } m>o\text{)} \quad (3.2.16)$$

Finally using equations (3.2.2), (3.2.9), (3.2.15) and (3.2.16) we obtain :

$$G(x,z;x',z') = \frac{j}{2kA} e^{-jk|z-z'|} + \frac{j}{A}\sum_{m=1}^{\infty} \frac{\cos\frac{m\pi x}{A}\cos\frac{m\pi x'}{A}}{k_m} e^{-jk_m|z-z'|} \quad (3.2.17)$$

In view of the absolute sign in the exponential, this expression holds everywhere.

Using the fact that

$$e^{-jk|z-z'|} = \cos k|z-z'| - j\sin k|z-z'|$$

we obtain

$$G(x,z;x',z') = \frac{j}{2kA}\cos k|z-z'| + \frac{1}{2kA}\sin k|z-z'| + \frac{j}{A}\sum_{m=1}^{\infty} \frac{\cos\frac{m\pi x}{A}\cos\frac{m\pi x'}{A}}{k_m} e^{-jk_m|z-z'|} \quad (3.2.18)$$

Thus,

$$G(x,z;\,x',\,z') = \frac{j}{2kA}\cos k|z-z'| + G'(x,z;\,x',\,z')$$

where $$G'(x,z;\,x',\,z') = \frac{1}{2kA}\sin k|z-z'| + \frac{j}{A}\sum_{m=1}^{\infty}\frac{\cos\frac{m\pi x}{A}\cos\frac{m\pi x'}{A}}{k_m}e^{-jk_m|z-z'|} \qquad (3.2.19)$$

$G'(x,z;\,x',\,z')$ given by equation (3.2.19) is real since only the TEM-mode was assumed to be propagating. So the expression given by (3.2.19) is to be used in the variational formulae (3.1.3) and (3.1.4).

Now let us make a coordinate transformation defined as follows :

$$x = u + \frac{A}{2} \qquad (3.2.20)$$

Hence the summation term in $G'(x,z;\,x',\,z')$ can be given by

$$\frac{j}{A}\sum_{m=1}^{\infty}\frac{\cos\frac{m\pi x}{A}\cos\frac{m\pi x'}{A}}{k_m}e^{-jk_m|z-z'|} = \frac{j}{A}\sum_{m=1}^{\infty}\frac{1}{k_m}\cos\frac{m\pi}{A}(u+\frac{A}{2})\cos\frac{m\pi}{A}(u'+\frac{A}{2})\,e^{-jk_m|z-z'|} \qquad (3.2.21)$$

$$= \frac{j}{A}\sum_{m=1}^{\text{odd}\,m}\frac{1}{k_m}\sin\frac{m\pi u}{A}\sin\frac{m\pi u'}{A}e^{-jk_m|z-z'|} + \frac{j}{A}\sum_{m=2}^{\text{even}\,m}\frac{1}{k_m}\cos\frac{m\pi u}{A}\cos\frac{m\pi u'}{A}e^{-jk_m|z-z'|} \qquad (3.2.22)$$

[Since cos (a+b) = cos a cos b - sin a sin b]

So, using equations (3.2.19) and (3.2.22) we obtain

$$G'(u,z;\,u',z') = \frac{1}{2kA}\sin k|z-z'| + \frac{j}{A}\sum_{m=1}^{\text{odd}\,m}\frac{1}{k_m}\sin\frac{m\pi u}{A}\sin\frac{m\pi u'}{A}e^{-jk_m|z-z'|} + \frac{j}{A}\sum_{m=2}^{\text{even}\,m}\frac{1}{k_m}\cos\frac{m\pi u}{A}\cos\frac{m\pi u'}{A}e^{-jk_m|z-z'|} \qquad (3.2.23)$$

This expression for $G'(u,z;\ u',z')$ can also be used instead of $G'(x,z;\ x',z')$ in the variational formulae (3.1.3) and (3.1.4).

The expressions ψ_e and ψ_o in (3.1.3) and (3.1.4) are the incident wave functions in the even and odd case respectively.

Hence,

for even excitation : $\psi_e = \cos kz$ (field maximum at $z = o$)

for odd excitation : $\psi_o = \sin kz$ (field node at $z = o$)

3.3 Numerical Evaluation of the Variational Expression

The variational expressions (3.1.3) and (3.1.4) are of the general form

$$Z = \frac{\iint K(r)\, G'(r,r')\, K(r')\, dS\, dS'}{\left[\int \psi(r)\ K(r)\, dS\right]^2} \qquad (3.3.1)$$

where r and r' are the field point and the source point radius vectors respectively. The first step in the evaluation of such an expression is the expansion of the unknown source function $K(r)$ into a Fourier series.

$$K(r) = \Sigma A_n f_n(r) \qquad (3.3.2)$$

The f_n are the set of the expansion functions and the A_n are the as yet undetermined expansion coefficients. We now define D_{mn} and C_m as follows :

$$D_{mn} = \iint f_n(r)\ G'(r,r')\, f_m(r')\, dS\, dS' = D_{nm} \qquad (3.3.3)$$

$$C_m = \int \psi(r)\ f_m(r)\, dS \qquad (3.3.4)$$

Then equation (3.3.1) can be written in general terms as :

$$\left(\sum_m A_m C_m\right)^2 Z = \sum_{m,n} A_m\ A_n\ D_{mn} \qquad (3.3.5)$$

Since the variational expression for Z is stationary with respect to the source function $K(r)$, the first derivative of Z with respect to any of the coefficients A_m must be zero. Thus, differentiating with respect to A_m we obtain from equation (3.3.5) :

$$2 C_m \left(\sum_m A_m C_m \right) Z + \left(\sum_m A_m C_m \right)^2 \frac{\partial Z}{\partial A_m} = 2 \sum_n A_n D_{mn}$$

$$\text{for all } m \qquad (3.3.6)$$

$$\text{or, } \sum_n A_n \left(\frac{D_{mn}}{C_m} - Z C_n \right) = 0 \quad \text{for all } m \qquad (3.3.7)$$

This expression can be solved by defining new coefficients B_m by

$$A_m = Z \left(\Sigma A_k C_k \right) B_m \qquad (3.3.8)$$

Multiplying through by C_m and summing we get

$$\sum_m A_m C_m = \sum_m Z \left(\Sigma A_k C_k \right) B_m C_m$$

$$\text{or} \quad Z = \frac{1}{\sum_m B_m C_m} \qquad (3.3.9)$$

By substituting equation (3.3.8) into equation (3.3.7), we obtain then m inhomogeneous linear equations,

$$\sum_n Z \left(\Sigma A_k C_k \right) B_n \left(\frac{D_{mn}}{C_m} - Z C_n \right) = 0 \quad \text{for all } m$$

$$\text{or, } \sum_n B_n \left(\frac{Dmn}{C_m} - Z C_n \right) = 0 \quad \text{for all } m$$

$$\text{or} \quad \sum_n B_n D_{mn} - Z C_m \sum_n B_n C_n = 0 \quad \text{for all } m$$

$$\text{or, } \sum_n D_{mn} B_n = C_m \quad \text{for all } m \qquad (3.3.10)$$

Since D_{mn} and C_m are known, the coefficients B_m can be evaluated on a computer. The impedance Z can then be found from equation (3.3.9).

Now we have all the expressions needed for the evaluation of the parameters of the equivalent circuit, except the current distribution functions $K(x', z')$. Since the impedance expressions are stationary with respect to $K(x', z')$, we will obtain fairly good values for the impedances by assuming rather simple current distribution functions.

We shall now deal with two special kinds of discontinuity, namely, thin transverse obstacles and circular cylindrical metallic posts.

CHAPTER 4

Equivalent Circuit Parameters of Thin Transverse Obstacles

By virtue of the stationary nature of the variational expressions (3.1.3) and (3.1.4) with respect to the source functions, second order approximations for the even and odd impedances are obtained when the source functions K_e and K_o are correct to the first order.

From the equivalent circuit of the obstacle in Fig. 3.2 it can be deduced that the odd excitation of the discontinuity is equivalent to placing an electric wall (short circuit) into the z = 0 plane. Since the thin transverse obstacle is entirely confined to the z = 0 plane, the total input impedance of the bisected equivalent circuit must be equal to zero in the odd case, thus

$$Z_{11} - Z_{12} = 0$$

which means $Z_{11} = Z_{12}$

Therefore, only the even case remains to be evaluated.

Hoefer and James [20] and Hoefer [19] have dealt with the problem of scattering on thin transverse obstacles in microstrip, using variational techniques. But they have used very approximate expressions for the current distribution function. They assumed a constant current distribution over the obstacle, i.e $K_e(x', z') = 1$. We shall work out the problem with more stringent assumptions for the current distribution. We shall choose upto three terms in the Fourier expansion of the source function and assume the distribution to be cosine in nature. We shall first give very briefly the results of Hoefer and James and then the detailed evaluation of the equivalent circuit parameters with higher terms for K_e will be given. We should mention here that in the papers of

Hoefer and James, a factor of 2 has been omitted in the final result. In the present derivation, this omission has been corrected.

4.1 Evaluation of $Z_{11} + Z_{12}$ with constant current distribution over the obstacle surface.

Let the current density $K_e(x', z')$ be constant and equal to one over the whole obstacle surface.

$$K_e(x', z') = 1 \tag{4.1.1}$$

Let us first evaluate the denominator of equation (3.1.3). Since $\psi_e(x,z) = \cos k z = 1$ on the obstacle surface, the integral in the denominator becomes

$$\int_{\text{obs.}} K_e(x,z)\, \psi_e(x,z)\, dS = \int_{\frac{A-d}{2}}^{\frac{A+d}{2}} 1.1.\, dx + \int_{\frac{A+d}{2}}^{\frac{A-d}{2}} 1.1.(-dx) = 2d \tag{4.1.2}$$

where d is the width of the obstacle. And the denominator is equal to $4d^2$.

By introducing the Green's function (3.2.19) and the approximate source function $K_e(x', z')$ into the numerator of equation (3.1.3), we obtain after integration over both sides of the obstacle and with some algebra ($z = z' = 0$):

$$Z_{11} + Z_{12} = 2Z = -2 \sum_{m=2}^{\text{even } m} \left(\frac{2}{m\pi}\right)^2 \left(\frac{A}{d}\right)^2 \frac{k}{k_m} \sin^2\left(\frac{m\pi}{2} \frac{d}{A}\right) \tag{4.1.3}$$

The equivalent circuit of the obstacle is thus a shunt inductance $Z = jx$ since k_m is positive imaginary for all higher modes.

4.2 Evaluation of $Z_{11} + Z_{12}$ with two terms in the current distribution over the obstacle surface.

As a more realistic assumption for the current distribution over the obstacle surface, we now consider two terms in the Fourier expansion of K(r) given by equation (3.3.2). Taking the current distribution to be cosine in nature, we can write

$$K_e(u,z) = A_0 + A_1 \cos \frac{\pi u}{d} \qquad (4.2.1)$$

where we have made the co-ordinate transformation

$$x = u + \frac{A}{2}$$

as we have shown in equation (3.2.20).

Now we must determine D_{mn} and C_m for this case.
From the definition of D_{mn} as given in equation (3.3.3), we can write

$$D_{12} = D_{21} = \int_{ob} \int_{ob} 1.\, G'(u,z\,;\, u',z') \cos \frac{\pi u'}{d}\, dS\, dS \qquad (4.2.2)$$

Inserting the expression for G' from equation (3.2.23) it can be shown that (for detailed calculations see Appendix A),

$$D_{12} = D_{21} = \sum_{m=2}^{\text{even}} j \frac{8d}{m k_m \pi^2 \left(1 - m^2 \frac{d^2}{A^2}\right)} \sin \frac{m\pi d}{A} \qquad (4.2.3)$$

Proceeding similarly, we obtain (see Appendix A),

$$D_{11} = \int_{obs} \int_{obs} G'(u,z;\, u',z')\, dS\, dS'$$

$$= \sum_{m=2}^{\text{even}} j \frac{16A}{k_m m^2 \pi^2} \sin^2 \frac{m\pi d}{2A} \qquad (4.2.4)$$

and, $$D_{22} = \int_{obs} \int_{obs} \cos \frac{\pi u}{d}\, G'(u,z;\, u',z') \cos \frac{\pi u'}{d}\, dS\, dS'$$

$$= \sum_{m=2}^{\text{even}} j \frac{16 d^2}{A k_m \pi^2 \left(1 - m^2 \frac{d^2}{A^2}\right)^2} \cos^2 \frac{m\pi d}{2A} \qquad (4.2.5)$$

Now from the definition of C_m given in equation (3.3.4) we would be able to calculate C_1 and C_2 as shown below.

$$C_1 = \int_{obs} \cos k z \cdot 1 \cdot dS$$

$$= \int_{obs} 1. \; 1. \; dS \qquad [\text{since } z = o \text{ on the obstacle}]$$

$$= \int_{-d/2}^{d/2} du + \int_{d/2}^{-d/2} (-du)$$

$$= 2d \qquad (4.2.6)$$

and $$C_2 = \int_{obs} \cos kz \; . \; \cos \frac{\pi u}{d} \, dS$$

$$= \int_{obs} 1. \; \cos \frac{\pi u}{d} \, dS$$

$$= \frac{d}{\pi} \left[\left(\sin \frac{\pi u}{d}\right)_{-d/2}^{d/2} + \left(-\sin \frac{\pi u}{d}\right)_{d/2}^{-d/2} \right]$$

$$= \frac{4d}{\pi} \qquad (4.2.7)$$

Since all the expressions for D_{mn}'s and C_m's are now known, $Z_{11} + Z_{12}$ can be found by using equations (3.3.9) and (3.3.10).

4.3 Evaluation of $Z_{11} + Z_{12}$ with three terms in the current distribution over the obstacle surface.

Let us now go a step further and calculate the input impedance with one more term in the Fourier expansion of the current distribution $K(r)$. We write

$$K_e(u, z) = A_0 + A_1 \cos \frac{\pi u}{d} + A_2 \cos \frac{2\pi u}{d} \qquad (4.3.1)$$

We have now to proceed exactly in the same way as we did for the case of two terms for $K_e(u,z)$. We have to find the expressions for the D_{mn}'s and C_m's. It is evident that the expressions for D_{12}, D_{11}, D_{22} and C_1 and C_2 remain the same as we have already calculated in section 4.2. We have now to find the expressions for the terms that arise due to the inclusion of the extra term $A_2 \cos \frac{2\pi u}{d}$ in the expression for $K_e(u,z)$. These can be given as follows. (For detailed calculations, see Appendix A).

$$D_{13} = D_{31} = \int_{obs} \int_{obs} 1.\ G'(u,z;u',z') \cos \frac{2\pi u'}{d}\, dS\, dS'$$

$$= \sum_{m=2}^{even} j \frac{16A}{k_m \pi^2 (4\frac{A^2}{d^2} - m^2)} \sin^2 \frac{m\pi d}{2A} \qquad (4.3.2)$$

$$D_{23} = D_{32} = \int_{obs} \int_{obs} \cos \frac{\pi u}{d}\, G'(u,z;u',z') \cos \frac{2\pi u'}{d}\, dS\, dS'$$

$$= \sum_{m=2}^{even} j \frac{8md}{k_m \pi^2 (1-m^2\frac{d^2}{A^2})(4\frac{A^2}{d^2} - m^2)} \sin \frac{m\pi d}{A} \qquad (4.3.3)$$

$$D_{33} = \int_{obs} \int_{obs} \cos \frac{2\pi u}{d}\, G'(u,z;u',z') \cos \frac{2\pi u'}{d}\, dS\, dS'$$

$$= \sum_{m=2}^{even} j \frac{16 m^2 A}{k_m \pi^2 (4\frac{A^2}{d^2} - m^2)^2} \sin^2 \frac{m\pi d}{2A} \qquad (4.3.4)$$

and $C_3 = \int_{obs} \cos kz \cdot \cos \frac{2\pi u}{d}\, dS \qquad [z = o]$

$$= \int_{-d/2}^{d/2} \cos \frac{2\pi u}{d}\, du + \int_{d/2}^{-d/2} \cos \frac{2\pi u}{d}\, (-du)$$

$$= 0 \qquad (4.3.5)$$

With the expressions for D_{mn}'s and C_m's, it is possible to evaluate $Z_{11} + Z_{12}$ with the help of equations (3.3.9) and (3.3.10).

Figure 9.2 shows, for comparison, the impedance of the obstacles as obtained with one, two and three terms in the obstacle current distribution function.

It is evident that considering more than one term in the current distribution is a definite improvement over the assumption of constant current distribution over the obstacle surface. But the results obtained by considering two and three terms for current distribution are almost identical. With each extra term considered for the current distribution function the amount of theoretical calculations involved increase drastically, whereas the increase in the accuracy of the final result is almost insignificant. So, we can say that for the determination of impedance parameter, we need not consider more than two terms in the current distribution function.

CHAPTER 5

Equivalent Circuit Parameters of Circular Cylindrical Metallic Posts

In the previous chapter, where the case of thin transverse obstacles was dealt with, due to the nature of the obstacle only the even impedance was needed to be calculated. But, in the present case of circular cylindrical metallic posts, shown in Figure 5.1, the input impedance for odd mode bisected equivalent circuit (of Figure 3.2) is not zero, This means Z_{11} and Z_{12} are different and hence both odd and even impedances have to be found . Since the calculations are quite involved, we shall restrict ourselves to considering only one term for the current distribution functions K_e and K_o.

5.1 Evaluation of $Z_{11} + Z_{12}$

Let us assume that the current in the even case is everywhere the same on the obstacle. We choose for convenience :

$$K_e(x', z') = \frac{1}{2\pi R} \quad \text{where } R = \text{radius of the cylindrical obstacle} \tag{5.1.1}$$

(The dimension of K_e does not matter in the variational expression)
The denominator of equation (3.1.3) is evaluated first

$$\int_{\text{obstacle}} K_e(x, z)\, \psi_e(x, z)\, dS = \int_{\text{obstacle}} \frac{1}{2\pi R}\, \psi_e(x, z)\, dx dz = \int_0^{2\pi} \frac{1}{2\pi R}\, \psi_e(x, z)\, R d\nu$$

$$= \frac{1}{2\pi} \int_0^{2\pi} \psi_e(x, z)\, d\nu \tag{5.1.2}$$

Using the representation of the field in terms of cylindrical wave functions, we apply the following lemma for the integration of $\psi_e(x, z)$ over the cylindrical obstacle:

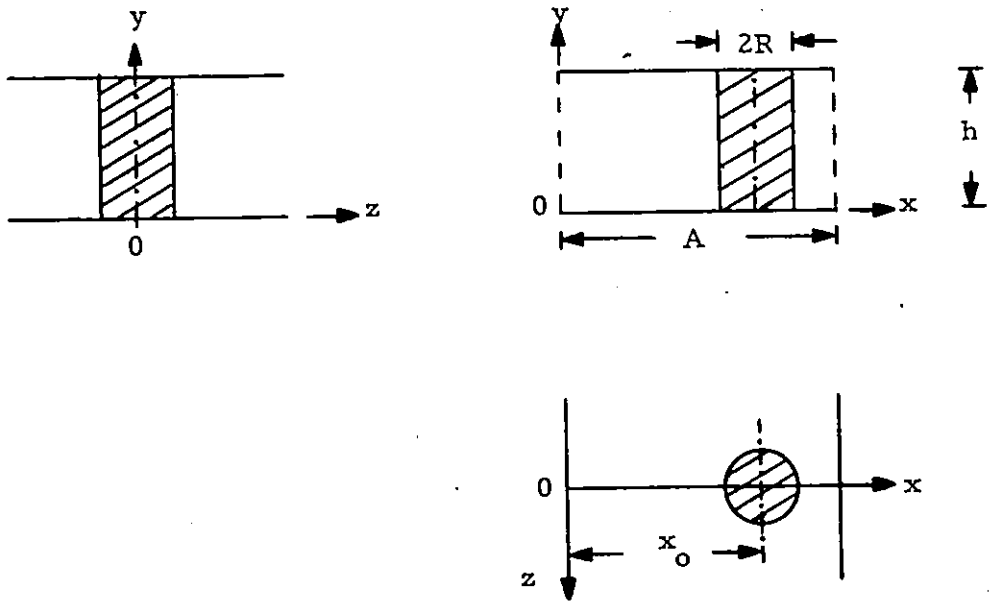

Figure 5.1 Circular cylindrical metallic post in a microstrip model.

Lemma: If $u(x, z) = u(r, \nu)$ is any solution of the two-dimensional source free wave equation inside a circle of radius r, then

$$\frac{1}{2\pi} \int_0^{2\pi} u(r,\nu)\, e^{jm\nu} d\nu = j^m J_m(kr)\, e^{jmD}\, u(o) \qquad (5.1.3)$$

where e^{jmD} is an operator defined by

$$\cos D = \frac{1}{jk} \frac{\partial}{\partial z} \quad ; \quad \sin D = \frac{1}{jk} \frac{\partial}{\partial x} \qquad (5.1.4)$$

and $e^{jmD}u(o)$ is the value of $e^{jmD}\, u(x, z)$ at the centre of the circle [21], [22].

Applying this lemma to equation(5.1.2), setting m = 0 and $\psi_e = \cos kz$ we obtain,

$$\int K_e(x,z)\, \psi_e(x,z)\, dS = J_o(kR) \cos k(z = o) = J_o(kR) \qquad (5.1.5)$$

and the denominator of equation(3.1.3) is thus $[J_o(kR)]^2$.

The lemma cannot be applied directly to the evaluation of the numerator because $G'(x, z; x', z')$ is not a solution of the source free wave equation. We proceed therefore as follows :

The field in the infinite waveguide can be considered as the superposition of the direct source field in infinite space plus the fields of an infinite number of image sources situated outside the waveguide [21] If we therefore subtract from the total source field $G'(x, z; x', z')$ the corresponding Green's function in free space, the difference is a solution of the homogeneous wave equation in the waveguide, and we can therefore apply the lemma. The Green's function in free space is [21]

$$G_s(r, r') = -\frac{1}{4} N_o \{(k)\, |r - r'|\} \qquad (5.1.6)$$

And the Green's function in the waveguide is thus

$$G'(x, z; x', z') = \{G'(x, z; x', z') - G_s(r, r')\} + G_s(r, r')$$

$$= \Gamma(x, z; x', z') + G_s(r, r') \qquad (5.1.7)$$

With this expression, the numerator in (3.1.3) becomes

$$\int\int \frac{1}{2\pi R}\left[\Gamma(x,z;x',z') + G_s(r,r')\right]\frac{1}{2\pi R}\,dx\,dz\,dx'dz'$$

$$= \int_0^{2\pi}\frac{1}{2\pi}\,d\nu\int_0^{2\pi}\frac{1}{2\pi}\,\Gamma(x,z;x',z')\,d\nu' + \int_0^{2\pi}\frac{1}{2\pi}\,d\nu\int_0^{2\pi}\frac{1}{2\pi}\,G_s(r,r')\,d\nu' \qquad (5.1.8)$$

The first term in this expression is evaluated using the lemma, and the second is immediately integrable, and we have at once :

$$\int_0^{2\pi}\frac{d\nu}{2\pi}\int_0^{2\pi}\frac{d\nu'}{2\pi}\,G'(x,z;x',z') = J_o^2(kR)\left\{\lim_{\substack{x\to x_o\\ z\to o}}\Gamma(x,z;x_o,o) - \frac{1}{4}\frac{N_o(kR)}{J_o(kR)}\right\} \qquad (5.1.9)$$

Thus, from (5.1.9) and (5.1.5)

$$Z_{11} + Z_{12} = 2jkA\left[\lim_{\substack{x\to x_o\\ z\to o}}\Gamma(x,z;x_o,o) - \frac{1}{4}\left\{N_o(kR)\,/\,J_o(kR)\right\}\right] \qquad (5.1.10)$$

The last step is the evaluation of $\lim \Gamma$. To do this let us write again the expression for $G'(x,z;x_o,o)$ (equation 3.2.19)

$$G'(x,z;x_o,o) = \frac{1}{2Ak}\sin k|z| + \frac{1}{A}\sum_{m=1}^{\infty}\frac{\cos\frac{m\pi x}{A}\cos\frac{m\pi x_o}{A}}{\sqrt{\left(\frac{m\pi}{A}\right)^2 - k^2}}\,e^{-\sqrt{\left(\frac{m\pi}{A}\right)^2 - k^2}\,|z|} \qquad (5.1.11)$$

where we have suitably manipulated the argument under the square root sign.

Let us now write G' in the form

$$G'(x,z;x_o,o) = \frac{1}{2Ak}\sin k|z| + \frac{1}{\pi}\sum_{m=1}^{\infty}\frac{\cos\frac{m\pi x}{A}\cos\frac{m\pi x_o}{A}}{m}\,e^{-\left(\frac{m\pi}{A}\right)|z|}$$

$$+ \frac{1}{\pi}\sum_{m=1}^{\infty}\cos\frac{m\pi x}{A}\cos\frac{m\pi x_o}{A}\left\{\frac{e^{-\frac{\pi}{A}|z|\sqrt{m^2 - \left(\frac{kA}{\pi}\right)^2}}}{\sqrt{m^2 - \left(\frac{kA}{\pi}\right)^2}} - \frac{e^{-\left(\frac{m\pi}{A}\right)|z|}}{m}\right\} \qquad (5.1.12)$$

Let us now write

$$\cos\frac{m\pi x}{A}\cos\frac{m\pi x_o}{A} = \frac{1}{2}\,\mathrm{Re}\left\{e^{j\frac{m\pi}{A}(x-x_o)} + e^{j\frac{m\pi}{A}(x+x_o)}\right\} \qquad (5.1.13)$$

Thus the second term of $G^1(x, z; x_o, o)$ becomes

$$\frac{1}{\pi}\sum_{m=1}^{\infty}\frac{1}{2}\,\mathrm{Re}\left\{\frac{e^{j\frac{m\pi}{A}(x-x_o)-\frac{m\pi}{A}|z|}}{m} + \frac{e^{j\frac{m\pi}{A}(x+x_o)-\frac{m\pi}{A}|z|}}{m}\right\}$$

$$= -\frac{\mathrm{Re}}{2\pi}\ln\left\{1-e^{j\frac{\pi}{A}(x-x_o)-\frac{\pi}{A}|z|}\right\} - \frac{\mathrm{Re}}{2\pi}\ln\left\{1-e^{j\frac{\pi}{A}(x+x_o)-\frac{\pi}{A}|z|}\right\} \qquad (5.1.14)$$

And we obtain for $\lim_{\substack{x\to x_o\\ z\to o}} \Gamma$:

$$\lim_{\substack{x\to x_o\\ z\to o}} \Gamma(x, z; x_o, o) = \frac{1}{\pi}\sum_{m=1}^{\infty}\cos^2\frac{m\pi x_o}{A}\left(\frac{1}{\sqrt{m^2-\left(\frac{kA}{\pi}\right)^2}} - \frac{1}{m}\right)$$

$$-\frac{1}{2\pi}\ln\left(2\sin\frac{\pi}{A}x_o\right) - \lim_{\substack{x\to x_o\\ z\to o}}\left\{\frac{\mathrm{Re}}{2\pi}\ln\left(1-e^{j\frac{\pi}{A}(x-x_o)-\frac{\pi}{A}|z|}\right)\right.$$

$$\left. - \frac{1}{4}N_o(k|r|)\right\} \qquad (5.1.15)$$

But $N_o(kr) \to \frac{2}{\pi}\ln\frac{\gamma k r}{2}$ where $\gamma = 1.781072$

and $\frac{\mathrm{Re}}{2\pi}\ln\left(1-e^{j\frac{\pi}{A}(x-x_o)-\frac{\pi}{A}|z|}\right) \to \frac{\mathrm{Re}}{2\pi}\ln\left(j\frac{\pi}{A}(x-x_o)-\frac{\pi}{A}|z|\right) = \frac{1}{2\pi}\ln\frac{\pi}{A}r$

(5.1.16)

So that

$$\lim_{\substack{x\to x_o\\ z\to o}} \Gamma(x, z; x_o, o) = \frac{1}{2\pi}\ln\left[\frac{\gamma k A}{4\pi\sin\frac{\pi}{A}x_o}\right] + \frac{1}{\pi}\sum_{m=1}^{\infty}\cos^2\frac{m\pi x_o}{A}\left(\frac{1}{\sqrt{m^2-\left(\frac{kA}{\pi}\right)^2}} - \frac{1}{m}\right)$$

(5.1.17)

And thus

$$Z_{11}+Z_{12}=2jkA\left[\frac{1}{2\pi}\ln\left(\frac{\gamma kA}{4\pi \sin\frac{\pi}{A}x_o}\right)+\frac{1}{\pi}\sum_{m=1}^{\infty}\cos^2\frac{m\pi x_o}{A}\left(\frac{1}{\sqrt{m^2-\left(\frac{kA}{\pi}\right)^2}}-\frac{1}{m}\right)\right.$$
$$\left.-\frac{1}{4}\left(N_o(kR)\ /\ J_o(kR)\right)\right] \qquad (5.1.18)$$

The last term can again be expanded as (to a first approximation)

$$-\frac{1}{4}\left(N_o(kR)\ /J_o(kR)\right) = -\frac{1}{2\pi}\left\{\ln\frac{\gamma kR}{2}+\frac{1}{4}(kR)^2\right\} \qquad (5.1.19)$$

And finally, the expression for $Z_{11}+Z_{12}$ becomes

$$Z_{11}+Z_{12}=2j\frac{A}{\lambda_t}\left[\ln\left(\frac{A}{R}\frac{1}{2\pi \sin\frac{\pi}{A}x_o}\right)-\frac{1}{4}(kR)^2+2\sum_{m=1}^{\infty}\cos^2\frac{m\pi x_o}{A}\left(\frac{1}{\sqrt{m^2-\left(\frac{kA}{\pi}\right)^2}}-\frac{1}{m}\right)\right]$$
$$(5.1.20)$$

5.2 Evaluation of $Z_{11} - Z_{12}$

In the odd case we assume that the current K_o is approximately given by

$$K_o = \frac{1}{2\pi R}\cos\nu \qquad (5.2.1)$$

where the angle ν is measured from the positive z-axis. This function is odd about the $z = 0$ plane.

We evaluate the denominator of equation(3.1.4) using the lemma:

$$\int K_o(x,z)\,\psi_o(x,z)\,dx\,dz = \int_0^{2\pi}\frac{1}{2\pi}\sin kz\cos\nu\,d\nu = jJ_1(kR)\frac{1}{jk}\frac{\partial}{\partial z}(\sin kz)\Big|_{z=o}$$
$$= J_1(kR)\cdot\cos kz\Big|_{z=o} = J_1(kR) \qquad (5.2.2)$$

Thus, the denominator of equation(3.1.4)is equal to $[J_1(kR)]^2$

In order to apply the lemma to the evaluation of the numerator, we proceed in the same way as in section 5.1.

We write

$$\int_0^{2\pi} \frac{d\nu}{2\pi} \cos\nu \int_0^{2\pi} \cos\nu' G'(x,z;\, x',z') \frac{d\nu}{2\pi} =$$

$$\int_0^{2\pi} \frac{d\nu}{2\pi} \cos\nu \int_0^{2\pi} \frac{d\nu'}{2\pi} \cos\nu' \, G_s(r,r') + \int_0^{2\pi} \frac{d\nu}{2\pi} \cos\nu \int_0^{2\pi} \frac{d\nu'}{2\pi} \cos\nu' \, \Gamma(x,z;x',z') \tag{5.2.3}$$

We first evaluate the first term

$$\int_0^{2\pi} \frac{d\nu}{2\pi} \cos\nu \int_0^{2\pi} \frac{d\nu'}{2\pi} \cos\nu' \, G_s(r,r')$$

$$= -\frac{1}{4} \sum_{n=-\infty}^{\infty} N_n(kR)\, J_n(kR) \int_0^{2\pi} \frac{d\nu}{2\pi} \cos\nu \, e^{jn\nu} \int_0^{2\pi} \frac{d\nu'}{2\pi} \cos\nu' \, e^{-jn\nu'}$$

$$= -\frac{1}{8} J_1(kR)\, N_1(kR) \tag{5.2.4}$$

For the second term, we apply the lemma

$$\int_0^{2\pi} \frac{d\nu}{2\pi} \cos\nu \int_0^{2\pi} \frac{d\nu'}{2\pi} \cos\nu' \, \Gamma(x,z;\, x',z')$$

$$= J_1(kR) \frac{1}{k} \int_0^{2\pi} \frac{d\nu}{2\pi} \cos\nu \frac{\partial}{\partial z'} \Gamma(x,z;\, x',z') \Big|_{\substack{x'=x_o \\ z'=o}}$$

$$= -J_1^2(kR) \frac{1}{k^2} \lim_{\substack{x\to x_o \\ z\to o}} \left\{ \frac{\partial^2}{\partial z^2} \Gamma(x,z;\, x_o,o) \right\} \tag{5.2.5}$$

where we have used the fact that

$$\frac{\partial \Gamma(x,z;\, x',z')}{\partial z'} = -\frac{\partial}{\partial z} \Gamma(x,z;\, x',z') \tag{5.2.6}$$

Thus from equations (3.1.4) and (5.2.2) we have

$$Z_{11}-Z_{12} = -\frac{j}{2kA}\;\frac{J_1^2(kR)}{-\frac{1}{8}J_1(kR)N_1(kR)-J_1^2(kR)\frac{1}{k^2}\lim_{\substack{x\to x_o\\ z\to o}}\{(\frac{\partial^2}{\partial z^2})\Gamma(x,z;x_o,o)\}} \qquad (5.2.7)$$

This expression is too precise in view of the assumption of a cosinusoidal current distribution. The second term can be dropped in the denominator of (5.2.7) since it is of the order of R^2, while the first term is of the order of unity.

Thus:

$$Z_{11}-Z_{12} = -\frac{j}{2kA}\;\frac{1}{-\frac{1}{8}\frac{N_1(kR)}{J_1(kR)}} = j\,\frac{8}{2kA}\,\frac{J_1(kR)}{N_1(kR)}$$

$$\approx -j\,\frac{A}{2\lambda_t}\,\left(\frac{2\pi R}{A}\right)^2 \qquad (5.2.8)$$

Where we have used the approximations

$$N_1(kR) \approx -\frac{1}{\pi}\,\frac{2}{kR} \quad \text{and} \quad J_1(kR) \approx \frac{1}{2}\,kR$$

5.3 Effect of cosinusoidal field distribution over the cross-section of the circular post.

For the evaluation of the even impedance of the circular post, it was assumed that the magnetic field was homogeneous over the entire cross-sectional area occupied by the post. A more realistic assumption is that the field falls off as $\cos\frac{2\pi}{T}z$ towards both sides of z = o plane. So, we have to correct the stored energy by assuming that the magnetic field is lower than the maximum value and equal to the average of the magnetic field over the crosssection .

The magnetic field $\bar{H}$ in a circular crosssection of unit radius is shown in Figure 5.2. The coordinate system conforms to the one already chosen for the microstrip model. We can write,

$$\bar{H} = H_o \cos \frac{2\pi}{T} z \, \bar{u}_x \tag{5.3.1}$$

where $T = \frac{2\lambda_t}{d}$ = normalized wavelength

λ_t = guided wavelength on the microstrip

d = diameter of circular crosssection

$\bar{u}_x$ = unit vector in x-direction

H_o = amplitude of the magnetic field

The average value of the field over the cylindrical crosssection is given by

$$\bar{H} = \frac{\int\int_{\text{cr. sec. area}} H_o \cos \frac{2\pi}{T} z \, dx \, dz}{\text{cross sectional area}} \tag{5.3.2}$$

Due to circular symmetry, it is necessary to integrate in equation (5.3.2) over one quarter circle, only in the first quadrant. So,

$$\bar{H} = \frac{\int_0 \int_0^{\sqrt{1-z^2}} H_o \cos \frac{2\pi}{T} z \, dx \, dz}{\pi/4} \tag{5.3.3}$$

$$= \frac{4}{\pi} \int_0^1 H_o \sqrt{1-z^2} \cos \frac{2\pi}{T} \cdot z \, dz \tag{5.3.4}$$

The definite(bounded)integral in equation (5.3.4) is a constituent of an integral representation of the Bessel Function as follows [25].

$$J_1\left(\frac{2\pi}{T}\right) = 2 C_1 \int_0^1 \sqrt{1 - u^2} \cos \frac{2\pi}{T} u \, du \tag{5.3.5}$$

where $$C_1 = \frac{\pi}{T} \frac{1.}{\Gamma(\frac{1}{2}) \Gamma(\frac{3}{2})} \tag{5.3.6}$$

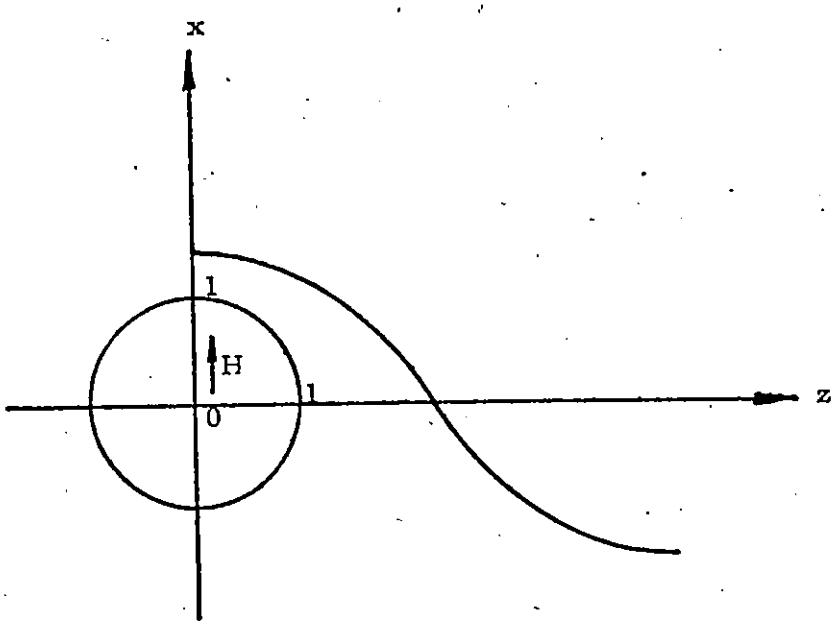

Figure 5.2 Magnetic field in a circular cross-section.

Thus, $$\int_0^1 \sqrt{1-u^2}\cos\frac{2\pi}{T}u\,du = \frac{J_1(\frac{2\pi}{T})}{2C_1} = \frac{J_1(\frac{2\pi}{T})}{\frac{2\pi}{T}}\Gamma(\tfrac{1}{2})\Gamma(\tfrac{3}{2}) \qquad (5.3.7)$$

Since $\Gamma(\frac{1}{2}) = \sqrt{\pi}$ and $\Gamma(\frac{3}{2}) = \frac{1}{2}\sqrt{\pi}$, we obtain from equations (5.3.4) and (5.3.7),

$$\bar{H} = \frac{4H_o}{\pi} \cdot \frac{J_1(\frac{2\pi}{T})}{\frac{2\pi}{T}} \cdot \frac{\pi}{2} \qquad (5.3.8)$$

or, in normalized form

$$\frac{\bar{H}}{H_o} = \frac{T}{\pi} J_1(\frac{2\pi}{T}) \qquad (5.3.9)$$

by replacing $T = \frac{2\lambda t}{\pi d} J_1(\frac{\pi d}{\lambda_t})$ (5.3.10)

To obtain more realistic values of the equivalent circuit parameters of a circular cylindrical post, we have to multiply the expressions obtained for even input impedance in equation (5.1.20) by $(\frac{\bar{H}}{H_o})^2$, For odd excitation, since fields of equal amplitude but opposite phase are incident on the circular cylindrical post, the correction does not apply.

CHAPTER 6

The Resonant Ring Method: Historical Background and its Potentials

The main difficulty in measuring the equivalent lumped circuit parameters of microstrip discontinuities resides in the elimination of the systematic errors introduced by the transitions which connect the microstrip section to equipments of the coaxial or waveguide type. Although techniques such as computer correction may be used to allow for this source of error, the basic problems of accurately measuring the transition and the reproducibility of the transition still remain. Moreover, computer correction techniques are quite expensive too. Such problems can be circumvented by testing discontinuities in a microstrip ring which may be coupled very loosely to the test equipment.

The technique of microstrip ring measurements have been demonstrated by several authors. Some experimental data have also been reported. We shall first survey some of these works briefly.

In 1969, P. Troughton [23] reported the technique of using a microstrip ring structure for the measurements of dispersion and wavelength in microstrip transmission line. The line was laid down on an Al_2O_3 substrate. He investigated the frequency range of 4 to 12 GHz. The ring resonator used, as shown in Figure 6.1, was at least five wavelengths long. He measured the wavelength of the propagating mode by noting the frequencies at which the ring resonated. Resonance occurs whenever the circumference of the ring equals an integer multiple of a wavelength at that frequency. No theory was given or suggested to explain the dispersive behaviour of the microstrip transmission lines. The experimental results showed that dispersion in microstrip is affected by both substrate thickness and strip width.

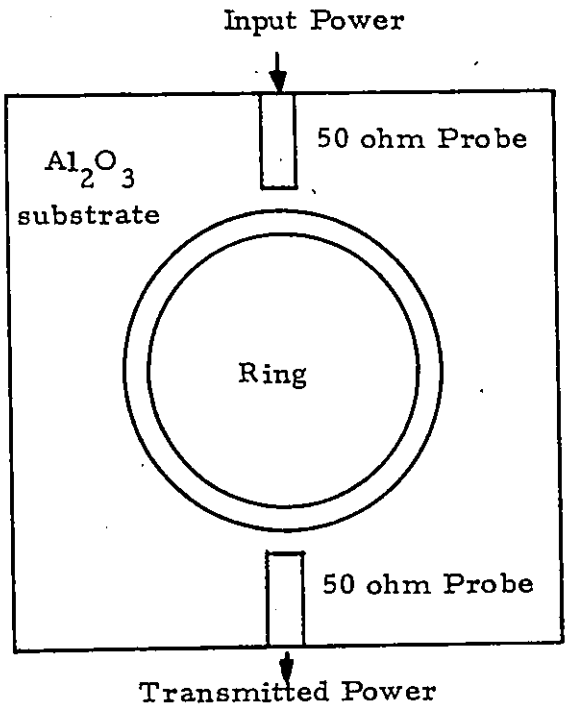

Figure 6.1 Plan view of microstrip resonator used by Troughton.

In 1971, Stephenson and Easter [10] used resonant ring techniques to characterize 90° bends in microstrip transmission line. They used both closed ring and open-ended resonators, as shown in Figure 6.2 for their work. Assuming the equivalent circuit of the 90° bends, as shown in Figure 6.3, the values for B/Y_o and equivalent electrical length ℓ_c have been given over the frequency range 1.6 - 11 GHz. The substrate used in their experiments is 0.5 mm of Lucalox.

In 1973, Douville and James [11] have studied the problem of 90° corners quite extensively, using a closed loop resonator as shown in Figure 6.4. The resonator contained four 90° bends. The equivalent circuit they chose was the same as was chosen by Stephenson and Easter. Over the frequency range 0.1 - 3 GHz, they have published results on the variation of equivalent length and shunt capacitance of 90° bends. The bends, that were studied, were mitred and unmitred and the substrates used were Rexolite and Stycast.

In 1975, Groll and Weidmann [12] used resonance methods to study different kinds of microstrip discontinuities. For an open ended microstrip line they have given results on the dependence of end capacitance on the width of the conductor. For a rectangular bend they have found the parameters of a lumped element T-equivalent circuit for a specific value of the line width. They have also studied the effect of an abrupt step of line width i.e an impedance step. They incorporated two microstrip lines of different widths in a ring resonator as shown in Figure 6.5 and have studied the variation of equivalent T- circuit parameters of the impedance step with the ratio of the physical widths of the two lines.

From the above it is evident that resonant ring techniques have enormous possibilities in the characterization of microstrip discontinuities. Until now all such measurements have been made to study

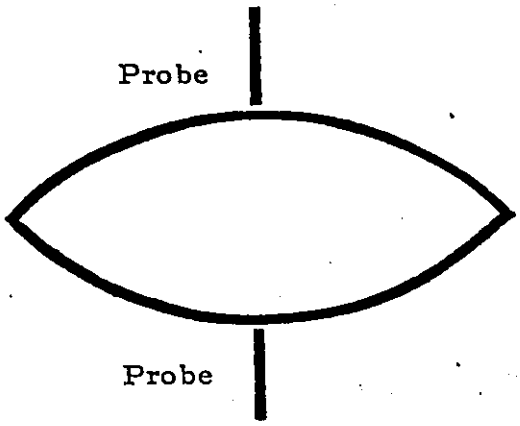

(a) Closed ring resonator including two 90 degree corners

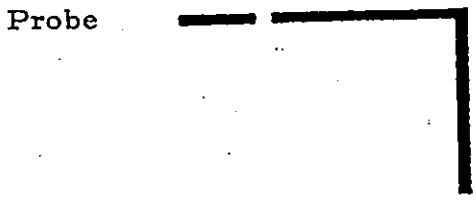

(b) Open-ended resonator including a 90 degree corner

Figure 6.2 Microstrip resonators used by Stephenson and Easter.

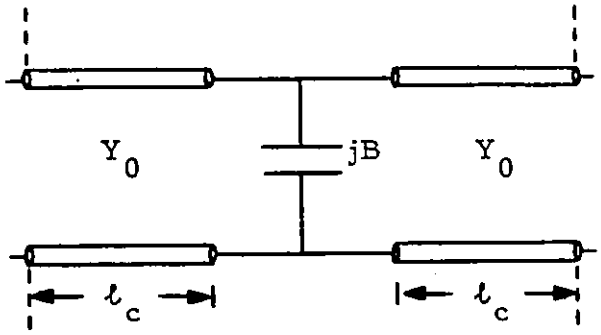

Figure 6.3 Equivalent circuit of 90 degree bends.

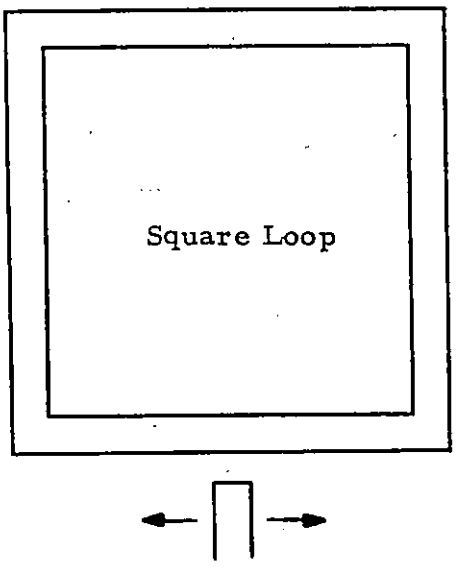

Figure 6.4 Square loop used by Douville and James.

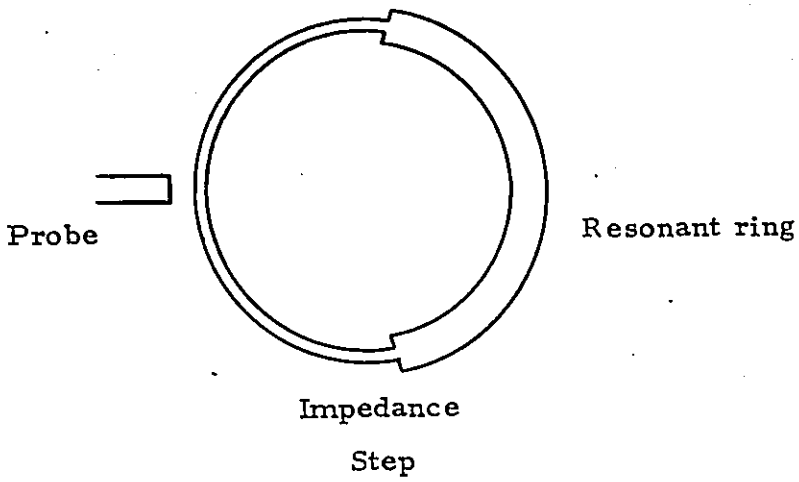

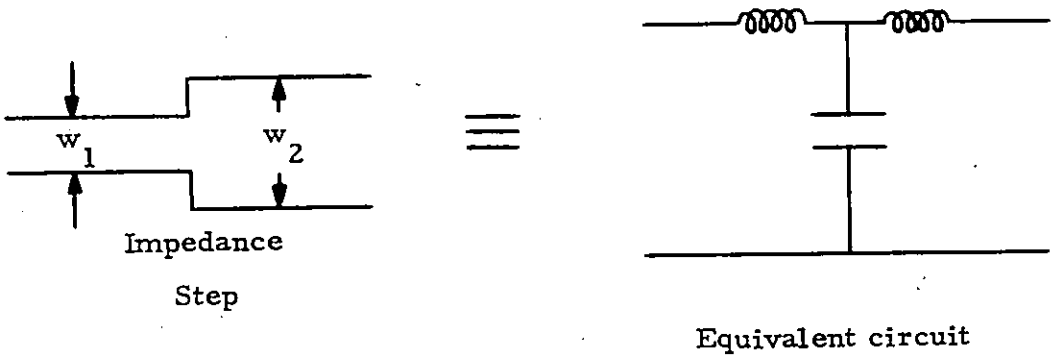

Figure 6.5 Ring resonator and the equivalent circuit used by Groll and Weidmann to study impedance steps.

some particular and specific types of discontinuities. We have developed [15,16] a comprehensive, general analysis of the microstrip ring containing a reciprocal discontinuity. The analysis has the potential to be used to find the Z-parameters of almost any reciprocal microstrip discontinuity, symmetrical as well as asymmetrical. In the next chapter we shall describe the analysis of the ring structure.

CHAPTER 7

Analysis of the Resonant Ring Containing A Reciprocal Discontinuity

A microstrip ring resonates if its electrical length is an integral multiple of the guided wavelength. When a discontinuity is introduced into the ring, each resonance degenerates into two distinct modes. This splitting is conveniently interpreted in terms of even and odd excitation of the discontinuity. The even case corresponds to the incidence of two waves of equal magnitude and phase upon the discontinuity, while in the odd case, waves of equal magnitude but opposite phase are incident from both sides. Either mode of resonance can be suppressed by an appropriate choice of the point of excitation along the ring.

7.1 Symmetrical discontinuities

If the discontinuity is symmetrical it can be represented by a symmetrical T or π section, in one single reference plane. This plane of electrical symmetry will henceforth be called $z = 0$ plane.

As has already been shown in Figure 3.2, the equivalent T-circuit of a symmetrical discontinuity can be divided into two identical half sections of zero electrical length. If the circuit is excited in the even mode, no current crosses the $z = 0$ plane. Therefore, the input impedance of each half section is not altered if the connections in this plane are cut. The normalized even input impedance at either port is thus $Z_{ie} = Z_{11} + Z_{12}$.

The normalized odd input impedance, in turn, is $Z_{io} = Z_{11} - Z_{12}$ and represents the impedance of a half-section which is short circuited in the $z = 0$ plane.

A. Lossless symmetrical discontinuities

The even and odd impedances of the discontinuity cause the shift in the resonance frequencies of the ring. This becomes evident if the (reactive) impedances are thought of as input impedances of fictitious transmission line sections which are open (even case) or short-circuited (odd case) at the other end. (Figures 7.1a and 7.1b).

The artificial increase of the electrical length of the ring resulting in the decrease of its resonance frequencies, is related to the normalized even and odd input impedances by the following expressions:

$$Z_{ie} = Z_{11} + Z_{12} = -j \cot k \ell_e \qquad \text{(even case)} \qquad (7.1.1)$$

$$Z_{io} = Z_{11} - Z_{12} = j \tan k \ell_o \qquad \text{(odd case)} \qquad (7.1.2)$$

$k = 2\pi/\lambda_t$, is the propagation constant of the quasi-TEM mode.

Figures 7.2a and 7.2b show the standing wave pattern on the ring resonating in the fundamental mode. For convenient presentation, the ring is cut open at z = 0 and straightened out. The fictitious lines representing Z_{ie} and Z_{io} have been added on either side.

Since at resonance, the total electrical length of the resonator (including the discontinuity) is $n \cdot \lambda_t$, where n is the harmonic number, the resonance conditions are

in the even case : $$\ell_{ring} + 2\ell_e = n\lambda_{te} \qquad (7.1.3)$$

in the odd case : $$\ell_{ring} + 2\ell_o = n\lambda_{to} \qquad (7.1.4)$$

ℓ_{ring} is the physical length of the ring along the mean circumference, and λ_{te} and λ_{to} are the guided wavelengths corresponding to the even and odd resonance frequency respectively. Since ℓ_{ring} is known and λ_t can be obtained from measurements, ℓ_e and [redacted] are determined from

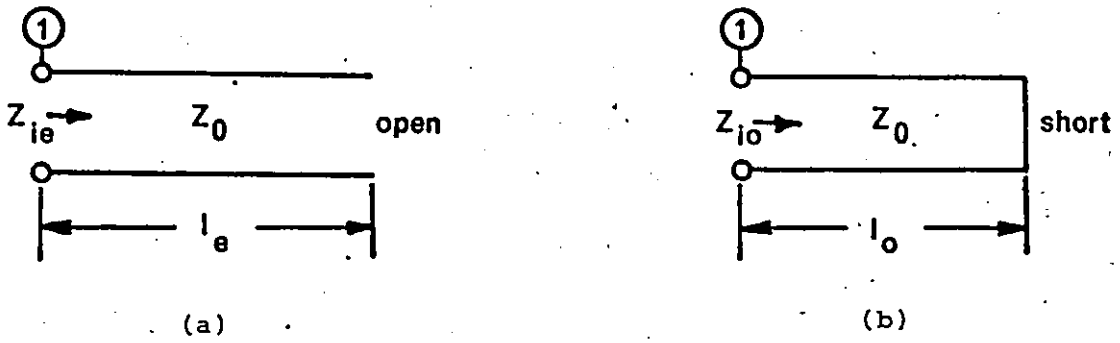

Figure 7.1 (a) Representation of the even input impedance Z_{ie} in plane 1 by a fictitious open-circuited line (lossless discontinuity).
(b) Representation of the odd input impedance Z_{io} in plane 1 by a fictitious short-circuited line (lossless discontinuity).

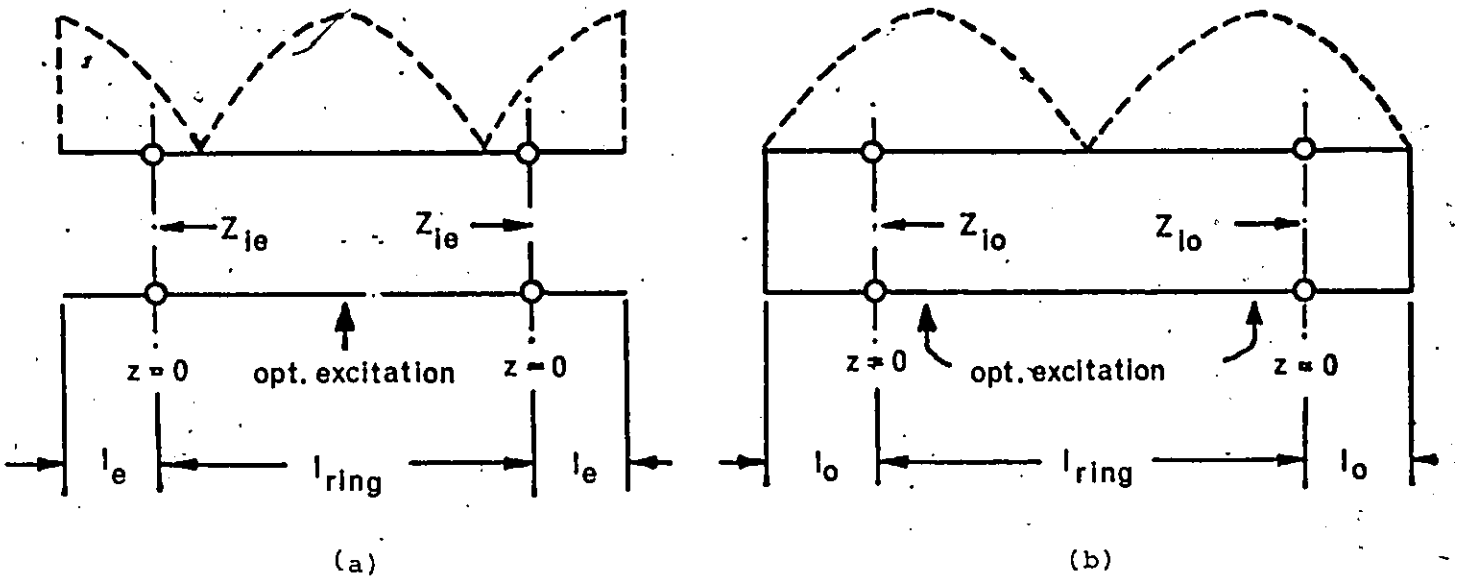

Figure 7.2 (a) Standing-wave pattern on the ring for even excitation of the discontinuity (n=1).
(b) Standing-wave pattern on the ring for odd excitation of the discontinuity (n=1).

equations (7.1.3) and (7.1.4). When introduced into equations (7.1.1) and (7.1.2) respectively, they yield

$$Z_{11} + Z_{12} = -j \cot \left[\frac{1}{2} k (n\lambda_{te} - \ell_{ring}) \right] = j \cot (\pi \frac{\ell_{ring}}{\lambda_{te}}) \quad (7.1.5)$$

$$Z_{11} - Z_{12} = j \tan \left[\frac{1}{2} k (n\lambda_{to} - \ell_{ring}) \right] = -j \tan (\pi \frac{\ell_{ring}}{\lambda_{to}}) \quad (7.1.6)$$

Since one measures resonance frequencies rather than wavelengths, it is more convenient to express λ_{te} and λ_{to} as follows :

$$\lambda_{te} = c / (f_{re} \sqrt{\varepsilon_{eff}(f_{re})}) \quad (7.1.7)$$

$$\lambda_{to} = c / (f_{ro} \sqrt{\varepsilon_{eff}(f_{ro})}) \quad (7.1.8)$$

and to introduce these expressions into equations (7.1.5) and (7.1.6) respectively. Thus

$$Z_{ie} = Z_{11} + Z_{12} = j \cot \frac{\pi \ell_{ring} \sqrt{\varepsilon_{eff}(f_{re})} f_{re}}{c} \quad (7.1.9)$$

$$Z_{io} = Z_{11} - Z_{12} = -j \tan \frac{\pi \ell_{ring} \sqrt{\varepsilon_{eff}(f_{ro})} f_{ro}}{c} \quad (7.1.10)$$

where $\varepsilon_{eff}(f)$ is the dispersive effective dielectric constant of the ring, c is the speed of light, f_{re} and f_{ro} are the even and odd resonance frequencies of the perturbed ring. These expressions form the basis for the measurement technique described later on.

B. Lossy symmetrical discontinuities

Dissipation and radiation losses render the Z-parameters of discontinuities complex. The complex even and odd input impedances of the equivalent circuit can be represented by sections of transmission lines terminated in a pure resistance (Figures 7.3a and 7.3b).

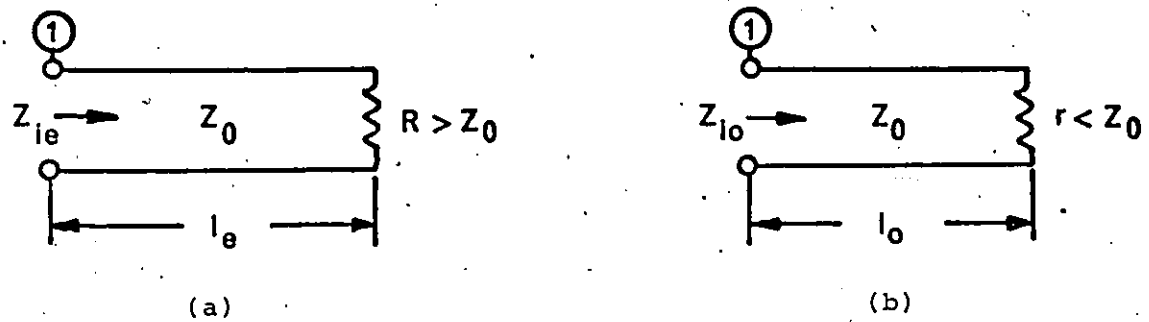

Figure 7.3 (a) Representation of the even input impedance Z_{ie} of a lossy discontinuity in plane 1 by a fictitious line terminated in $R>Z_0$.
(b) Representation of the odd input impedance Z_{io} of a lossy discontinuity in plane 1 by a fictitious line terminated in $r<Z_0$.

The terminating resistance must be larger than Z_o in the even case (voltage maximum at $z = 0$) and smaller than Z_o in the odd case (voltage minimum at $z = 0$). Note that for the lossless case, R tends towards ∞, while r becomes zero.

The lengths and terminations of the fictitious lines are such that (See Appendix B),

$$Z_{ie} = Z_{11} + Z_{12} = \frac{\frac{R}{Z_o} + j \tan k\ell_e}{1 + j\frac{R}{Z_o}\tan k\ell_e} = \frac{\frac{R}{Z_o} - j \tan\left(\frac{\pi \ell_{ring}}{\lambda_{te}}\right)}{1 - j\frac{R}{Z_o}\tan\left(\frac{\pi \ell_{ring}}{\lambda_{te}}\right)} \qquad (7.1.11)$$

$$Z_{io} = Z_{11} - Z_{12} = \frac{\frac{r}{Z_o} + j \tan k\ell_o}{1 + j\frac{r}{Z_o}\tan k\ell_o} = \frac{\frac{r}{Z_o} - j \tan\left(\frac{\pi \ell_{ring}}{\lambda_{to}}\right)}{1 - j\frac{r}{Z_o}\tan\left(\frac{\pi \ell_{ring}}{\lambda_{to}}\right)} \qquad (7.1.12)$$

The wavelengths λ_{te} and λ_{to} satisfy equations (7.1.7) and (7.1.8) respectively and are determined as in the lossless case. R and r affect the Q-factor of the ring.

Let Q_1 be the unloaded Q of the ring, while Q_{2e} and Q_{2o} are the loaded Q-factors of the ring for even and odd excitation of the discontinuity respectively. Then (see Appendix B),

$$\frac{R}{Z_o} = \frac{2}{\pi n}\,\frac{Q_1\, Q_{2e}}{Q_1 - Q_{2e}} \qquad (7.1.13)$$

$$\frac{r}{Z_o} = \frac{\pi n}{2}\,\frac{Q_1 - Q_{2o}}{Q_1\, Q_{2o}} \qquad (7.1.14)$$

where n is the harmonic number.

The circuit parameters Z_{11} and Z_{12} are determined from R, λ_{te}, r and λ_{to} using equations (7.1.11) and (7.1.12).

7.2 Unsymmetrical discontinuities

A. Lossless unsymmetrical discontinuities

Unsymmetrical lossless discontinuities shift the standing wave pattern along the ring. The amount of phase shift depends on the degree of unsymmetry. By shifting the point of even excitation, the resonant ring can be made an electrically symmetrical structure and the corresponding discontinuity does now appear as a cascade of the initial unsymmetrical discontinuity and additional length of line ℓ_a.

ℓ_a = 2 x displacement of the point of pure even excitation.

B. Lossy unsymmetrical discontinuities

The concept of even and odd excitation can only be applied to those lossy unsymmetrical discontinuities which can be transformed into a symmetrical two port by adding an appropriate length of line to one of their ports. In terms of S-parameters, this condition is fulfilled if

$$|S_{11}| = |S_{22}|$$

The Z-parameters in the plane of electrical symmetry are then calculated using equations (7.1.11) and (7.1.12).

CHAPTER 8

The Measurement Technique and Experimental Arrangement

8.1 Measurement Technique

It has been noted in Chapter 7 that for making the evaluation of discontinuity parameters, measurements of resonant frequencies and Q-factors are to be done. Resonant frequencies and Q-factors of the microstrip ring change due to the introduction of a discontinuity. So, the measurements are to be done in two stages.

i) The resonant frequencies and the unloaded Q-factors of the ring are measured before the discontinuity is introduced.

ii) The discontinuity is then introduced (either into the same ring or, if this is impractical, into another identical ring), and the even and odd resonant frequencies together with the corresponding loaded Q-factors of the structure are measured.

The ring should be as uniform as possible since even a small irregularity may introduce effects of the same order as the effects to be measured. The ring is best excited by a capacitive launcher which can be moved along the outer contour of the ring for about one quarter of its circumference to select the optimal point of excitation for each resonance. Coupling should be as light as the sensitivity of the measuring equipment permits. Even then, the launcher changes the resonant frequencies slightly. But as long as the measurements on the empty and the perturbed ring are made at the same coupling strength, the effect of the launcher is eliminated since it affects all measurements in the same way (see Chapter 10 for a proof of this).

Resonant frequencies can be determined from either reflection or transmission measurements. The former method has the advantage that only one coupling link between ring and peripheral equipment is required. Care must be taken to measure all resonant frequencies with the best possible accuracy since the discontinuity impedance values are very sensitive to frequency variations. This accuracy is limited by the sharpness of the resonance response rather than the performance of available counters for the microwave range.

Q-factors are best measured in the transmission mode [14] which, unfortunately, requires a second coupling link between ring and the peripheral equipment, but may be evaluated from reflection measurements with lesser accuracy.

Changes in temperature alter the resonant frequencies of the ring. In most cases, it will be necessary to stabilize the temperature of the substrate within $\pm$ 0.5° C if meaningful measurements are to be made.

8.2 Experimental Arrangement

A. The ring resonator

Measurements have been made in a ring which had the shape of a racetrack (Figure 8.1). The discontinuity could thus be placed into a straight section of line, and the launcher could also be moved along a straight line on the opposite side. The ring had a characteristic impedance of about 27 Ω (w/h=2.7) on a 5 mm Stycast substrate with a nominal dielectric constant of 10.6. The mean circumference of the ring was ℓ_{ring} = 59.124 cm for the measurements on metallic posts of circular cross-section and ℓ_{ring} = 57.375 cm for measurements on thin metallic obstacles. The oversize substrate was chosen to minimize errors due to dimensional inaccuracies.

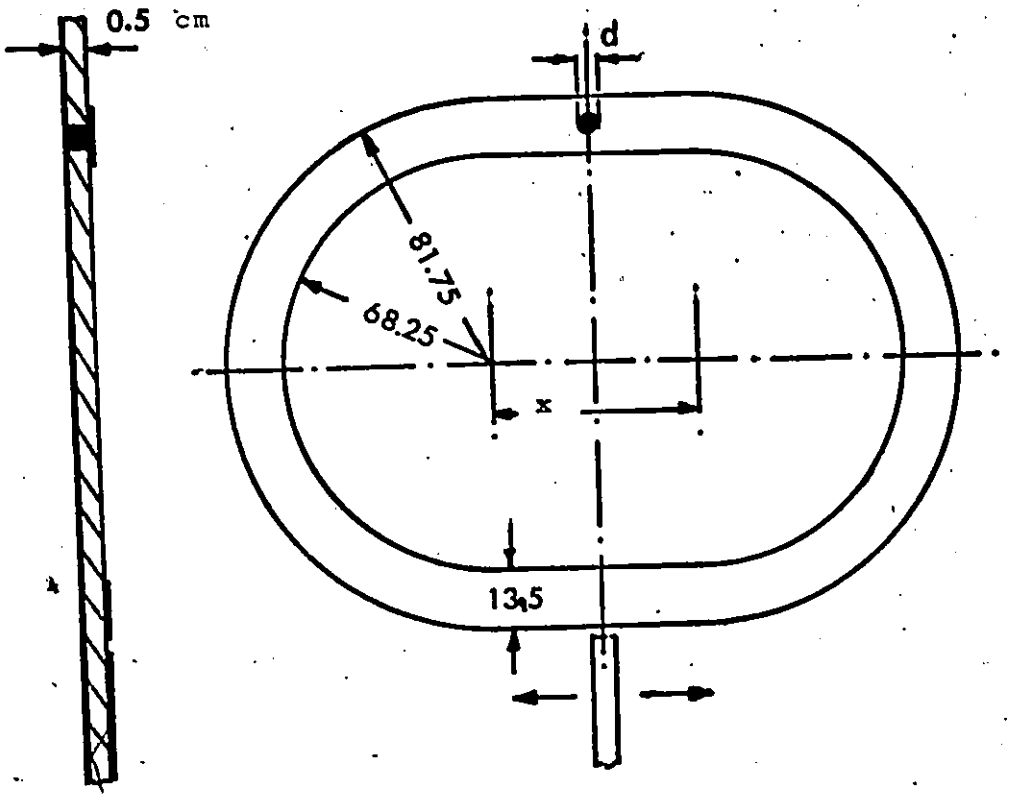

Figure 8.1 Microstrip ring used for measuring the Z parameters (dimensions in millimeters)

(a) x = 60 mm for centered metallic posts
(b) x = 51.25 mm for thin transverse obstacles.

B. The obstacles (discontinuities)

Two types of discontinuities have been investigated, namely very thin metallic plates and cylindrical metallic posts. These were chosen because of the ease of introduction of obstacles after measurements on the empty ring were made. In both these cases, the discontinuities were centered in the cross-section of the microstrip.

The thin metallic obstacles were made of strips of very thin copper sheets. These were introduced into the ring in the following way. The ring was cut open at the intended position of the obstacle. The thin metallic foil was introduced and then the ring was reassembled. For thin obstacles, only the even resonance measurements are to be made, and for even resonances no current crosses the $z = 0$ plane. Hence, cutting the ring open does not affect the measurements.

The metallic posts were realized by drilling holes across the microstrip and filling those with mercury.

In each case, good electrical contact was insured at the strip and the ground plane, and the electrical parameters of the discontinuity could be reproduced within the limits of accuracy of the equipment.

C. The Temperature Chamber

As has been already indicated in section 8.1, to make the measurements of discontinuity parameters, the temperature of the substrate has to be stabilized within $\pm$ 0.5°C. Otherwise the dielectric constant of the substrate shows fluctuations to an extent that makes meaningful measurements impossible. For reducing the fluctuation of temperature, a temperature controlled box was designed, and the ring was placed in it.

The box as shown in Figure 8.2, was lined inside by a 2.5 inch thick layer of styrofoam on all sides, which is a very good temperature isolator. Only the upper lid could be removed to place the microstrip

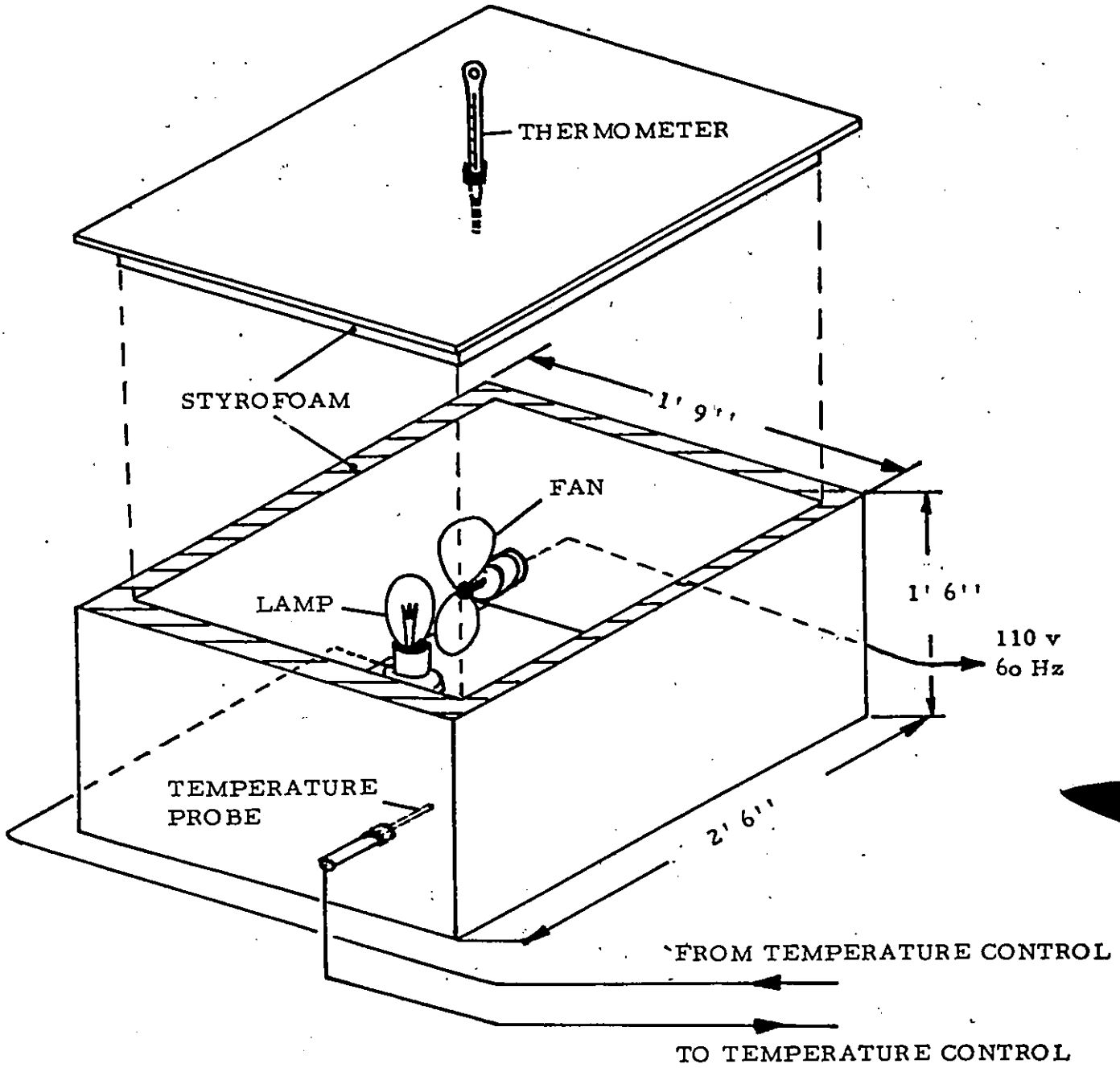

Figure 8.2 Temperature controlled box used for the stabilization of the temperature of the substrate.

ring inside the box. A cable was introduced into the box through a very small hole in one side of the box, and that served as the connection between the launcher for the ring and the peripheral equipment. By pulling or pushing the cable from outside, the launcher could be placed at the appropriate excitation points along the ring. A temperature probe and a heater element, connected to a temperature control equipment outside, was also mounted within the box. During the course of the experiments, the temperature control equipment was set at $30.5^{\circ}C$. The sensitivity of the equipment permitted the temperature within the box to be kept in the range $30.5^{\circ}C \pm 0.4^{\circ}C$. To insure that the whole temperature chamber was being heated uniformly, a small fan circulated the air in the box continuously. The temperature inside the box was constantly monitored with the help of a thermometer which was introduced through a very small hole in the top lid of the box.

D. The Measurement Procedure

The circuit for the measurement of the resonance frequencies was laid out as shown in Figure 8.3. The reflection characteristics of the resonant ring were measured using a network analyzer. The ring response was observed on a phase-magnitude display. A spectrum analyzer was used to compare the resonance frequencies of the ring with the frequency of a precision frequency generator. The output frequency of the generator was displayed on a digital frequency counter. The vertical output of the spectrum analyzer was fed to the network analyzer as the z-axis marker. (* See page 57)

Now we shall describe the procedure followed to determine accurately any particular resonant frequency. Initially the sweep oscillator was sweeping in Δf mode and the response of the ring was centered on the screen of the phase-magnitude display by adjusting the central frequency of the sweep. Then the sweep was changed to manual and the output frequency of the sweep oscillator was set as close to the peak as

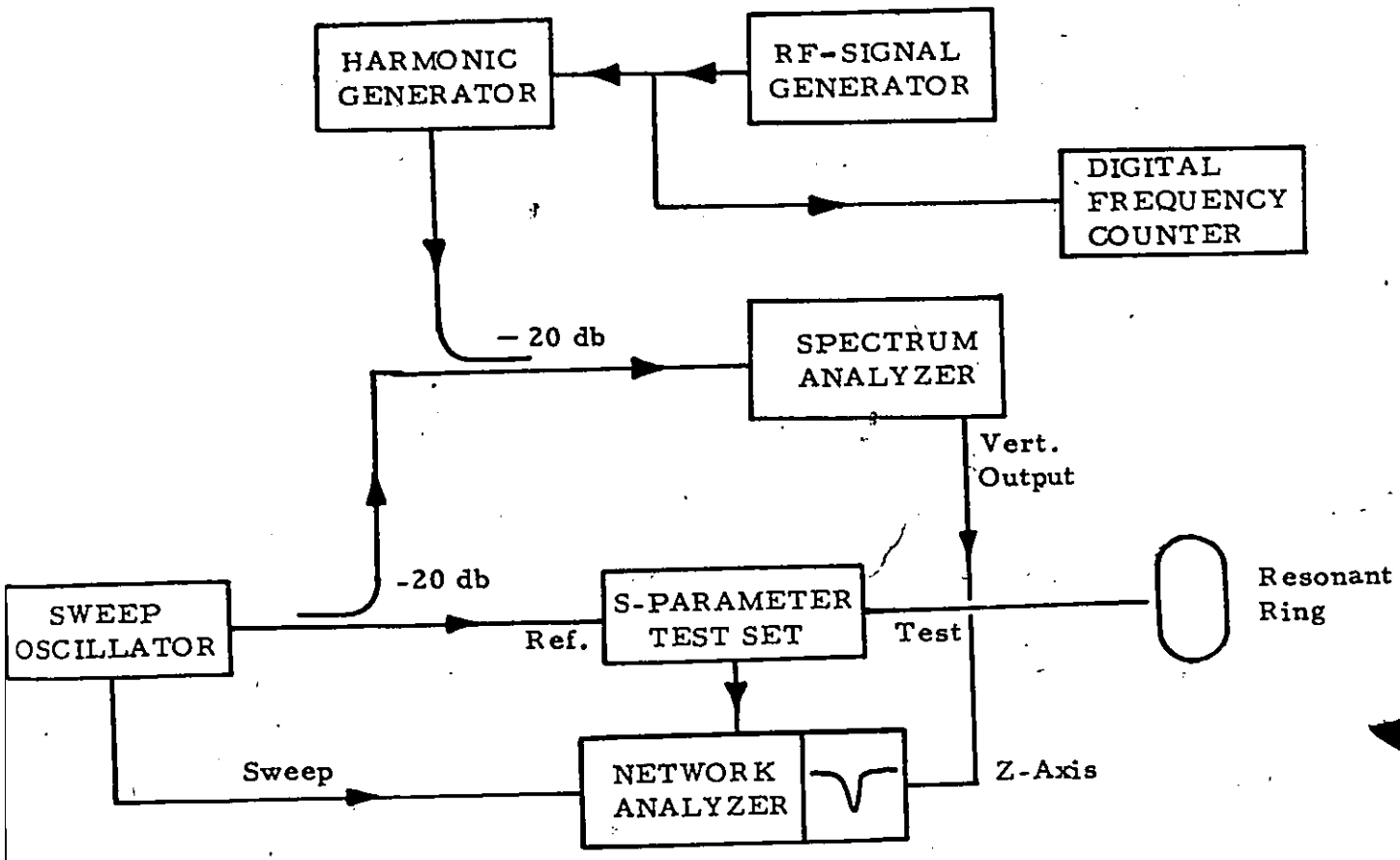

Figure 8.3 Circuit diagram for measuring the resonance frequencies of the microstrip ring.

possible. Now the local oscillator of the spectrum analyzer was adjusted and tuned such that the sweep oscillator frequency was in the centre of the spectrum analyzer screen. Then the scanning mode of the spectrum analyzer was changed to "manual". The sweeper was again swept in automatic mode at a very low speed. The vertical output of the spectrum analyzer density modulated the phase-magnitude display, producing a dot on the absorption curve very near to its peak. The frequency of the spectrum analyzer was now finally adjusted to place the dot exactly on the peak. Now the frequency of the r.f. signal generator output was adjusted. As soon as this frequency became identical with the centre frequency of the spectrum analyzer (which in turn was tuned to the ring resonant frequency), the intensity of the phase-magnitude display trace increased drastically over the whole sweeping range. Under this setting, the frequency of the r.f. signal generator output is the required resonance frequency of the ring.

The r.f. signal generator available for our experiments had a frequency range much smaller than the range (.1 - 2GHz) over which the ring resonances were being studied. This difficulty was avoided by inserting a harmonic generator unit between the r.f. signal generator and the spectrum analyzer. By properly choosing r.f. frequency and using its proper harmonics it was always possible to match any ring resonance frequency.

Measurements of frequencies of the peaks of absorption could be repeated within $\pm$ 20 KHz.

* Refer to the HP Network Analyzer and Spectrum Analyzer Operating Manuals for details referred to in the description of the experimental procedure.

CHAPTER 9

Theoretical and Experimental Results

The equivalent circuit parameters of two types of obstacles, namely thin transverse metallic obtacles and circular cylindrical metallic posts, have been calculated theoretically and determined experimentally. The results obtained using theoretical and experimental methods have been compared. These two types of discontinuities have been chosen because, while making the experimental investigation, they could easily be introduced into the ring after measurements on the empty ring were made.

Using the method of Lewin [24] we have theoretically studied the amount of losses due to radiation from transverse metallic obstacles (see Appendix D). It was evident that a very small portion of the power incident on the obstacle is radiated. For the experimental part, we tried to measure the 3-db line width of resonance and Q-factor for the determination of losses due to the discontinuities, The Q-factor of the ring was so little affected by the discontinuities that they appeared to be almost lossless, and the accuracy in determining the resistances R and r was unsatisfactory. They are therefore not reported here. (See also Appendix E)

9.1 Thin transverse metallic obstacles

It was shown in chapter 4 that in the case of a thin transverse obstacle, which is confined entirely in the $z = 0$ plane, the input impedance of the bisected equivalent circuit for odd excitation is zero and consequently $Z_{11} = Z_{12}$. This means that such obstacles may be determined by even excitation only.

We have experimentally determined (in the range .1 - 2 GHz) the equivalent Z-parameter of two thin transverse obstacles of widths d=1.62 mm and d = 3.07 mm. To do this, initially the resonant frequencies of the empty ring resonator (length = 57.375 cm) were determined. These

are shown in Table 9.1. From these frequency measurements, the corresponding effective dielectric constants for the substrate were found in the following way. If λ_t is the guided wavelength on the ring at the resonant frequency f_r, then ε_{eff} is given by

$$\varepsilon_{eff} = \frac{c^2}{\lambda_t^2 f_r^2} \qquad (9.1.1)$$

where $\lambda_t = \frac{\ell_{ring}}{n}$

n = harmonic number

and c = velocity of light

The effective dielectric constants at the different resonant frequencies of the ring are given in Table 9.2. This data have been plotted in Figure 9.1.

After determining ε_{eff} from empty ring resonant frequencies, two thin obstacles (d = 1.62 mm and d = 3.07 mm) were introduced into the ring one by one. For each obstacle introduced, the corresponding set of even resonant frequencies were measured. For each of these resonant frequencies, the corresponding ε_{eff} was determined. This was done in the following way,

Suppose f is an even resonant frequency of the ring with an obstacle introduced in it. Referring to Table 9.2, let f_u and f_ℓ be the two empty resonant frequencies just above and below f. Let the two ε_{eff} values corresponding to f_u and f_ℓ be ε_u and ε_ℓ respectively. So, by making linear interpolation, the effective dielectric constant ε corresponding to f will be

$$\varepsilon = \varepsilon_\ell + \frac{\varepsilon_u - \varepsilon_\ell}{f_u - f_\ell}(f - f_\ell) \qquad (9.1.2)$$

The even resonant frequencies with the obstacles and the corresponding

Table 9.1

Resonance Frequencies of the Empty Ring

(Stycast line, $\varepsilon_r = 10.6$, w/h = 2.7, h=5mm, Z_0=27ohms, $\ell_{ring} = 57.375$ cm)

Harmonic Number n	Resonant Frequency (M Hz)
1	193.331
2	386.523
3	575.756
4	762.799
5	947.170
6	1129.500
7	1309.884
8	1488.480
9	1664.636
10	1839.920
11	2013.838

Table 9.2

ε_{eff} at the Resonance Frequencies of the Empty Ring

(Stycast line, $\varepsilon_r = 10.6$, w/h= 2.7, h= 5 mm, $Z_0 = 27$ ohms, $\ell_{ring} = 57.375$ cm)

Harmonic No. n	Resonance Frequency (f_r) (MHz)	λ_t (cm)	ε_{eff}
1	193.331	57.375	7.28855
2	386.523	28.688	7.29556
3	575.756	19.125	7.39923
4	762.799	14.344	7.49373
5	947.170	11.475	7.60855
6	1129.500	9.563	7.69123
7	1309.884	8.196	7.78395
8	1488.480	7.172	7.87285
9	1664.636	6.375	7.97025
10	1839.920	5.738	8.05263
11	2013.838	5.216	8.13679

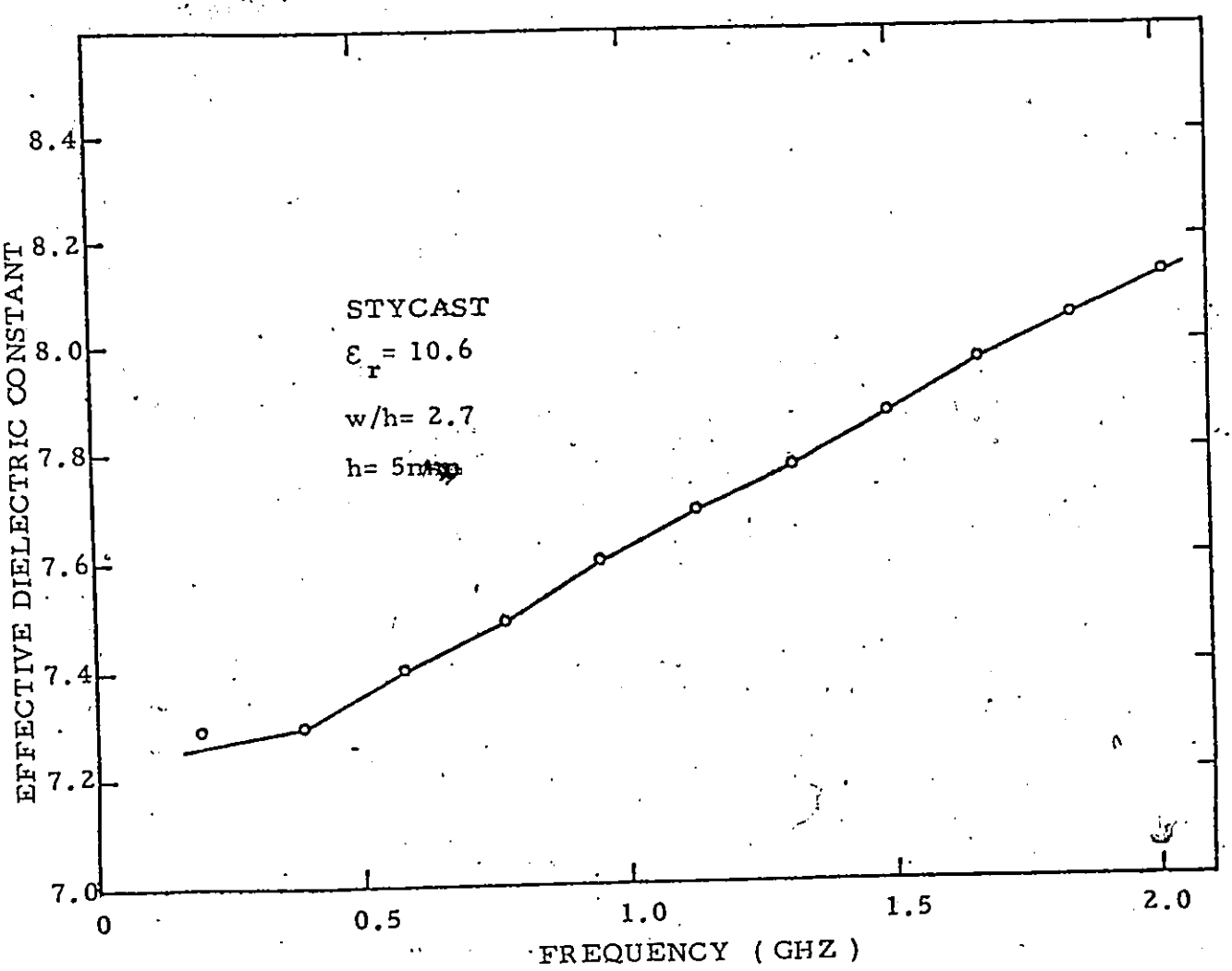

Figure 9.1 Measured effective dielectric constant for the microstrip ring. (ℓ_{ring}= 57.375 cm)

effective dielectric constants are given in Tables 9.3 and 9.4.

Once the even resonant frequencies of the ring resonator and the corresponding ε_{eff} values are known, the equivalent circuit parameter Z of the thin transverse obstacles are easily found with help of the equation (7.1.9).

$$Z = Z_{11} = Z_{12} = j \frac{1}{2} \cot \frac{\pi \ell_{ring} \sqrt{\varepsilon_{eff}(f_{re})}\, f_{re}}{c} \qquad (9.1.3)$$

The values of Z at different even resonant frequencies for the two thin transverse obstacles are given in Tables 9.5 and 9.6.

The equivalent circuit parameters for the same two thin transverse obstacles have also been found theoretically following the procedure described in Chapter 4. Z has been found out using one, two and three terms for the current distribution over the surface of the obstacle, namely

$$K_e(u,z) = A_o,\ A_o + A_1 \cos\frac{\pi u}{d},\ A_o + A_1 \cos\frac{\pi u}{d} + A_2 \cos\frac{2\pi u}{d}$$

To obtain the parameters of the microstrip model, the capacitance C_o per unit length of the line at d.c. was determined by a finite difference method developed at CRC, Ottawa. ε_{eff} for d.c. was also determined. Then the dispersive dielectric constant $\varepsilon_{eff}(f)$ was calculated using Jain's [27] microstrip model. Finally, the value of Z_o was found from C and $\varepsilon_{eff}(f)$ and A was obtained via the expression given in page 4. A was found to be 24.327 mm. The theoretical values obtained for Z for the two different obstacles are given in Tables 9.7 and 9.8.

The experimental and theoretical values of Z are compared in Figure 9.2 for the two thin transverse obstacle widths d = 1.62 mm and d = 3.07 mm.

It can be seen that the measured values for impedances form a reasonably smooth curve. The agreement between theoretical and experimental values of impedance is quite good for the lower frequencies.

Table 9.3

Even Resonance Frequency and ε_{eff} for

Obstacle Width d= 1.62 mm

(Stycast line, ε_r= 10.6, w/h= 2.7, h= 5 mm, Z_0= 27 ohms,

ℓ_{ring}= 57.375 cm)

Frequency (MHz)	ε_{eff}
272.205	7.29141
453.867	7.33231
634.692	7.42883
815.236	7.52174
994.279	7.61815
1172.034	7.71283
1348.419	7.80288
1523.640	7.89198
1697.852	7.98554
1870.088	8.06690

Table 9.4

Even Resonance Frequency and ε_{eff} for

Obstacle Width d= 3.07 mm

(Stycast line, ε_r= 10.6, w/h= 2.7, h= 5 mm, Z_0= 27 ohms,

ℓ_{ring}= 57.375 cm)

Frequency (MHz)	ε_{eff}
276.285	7.29155
459.256	7.33526
641.508	7.43227
821.963	7.52537
1001.990	7.62230
1180.038	7.71695
1355.664	7.80648
1531.384	7.89626
1705.924	7.98934
1876.676	8.07009

Table 9.5

Experimental Values of Equivalent Circuit Parameters for Obstacle Width d= 1.62 mm

(Stycast line, ε_r= 10.6, w/h= 2.7, h= 5 mm, Z_0= 27 ohms, ℓ_{ring}= 57.375 cm)

Frequency (MHz)	Z (normalized)
272.205	0.14983
453.867	0.24899
634.692	0.33541
815.236	0.41169
994.279	0.48704
1172.034	0.56018
1348.419	0.63623
1523.640	0.70905
1697.852	0.76153
1870.088	0.85223

Table 9.6

Experimental Values of Equivalent Circuit Parameters for Obstacle Width d= 3.07 mm

(Stycast line, ε_r= 10.6, w/h= 2.7, h= 5 mm, Z_0= 27 ohms, ℓ_{ring}= 57.375 cm)

Frequency (MHz)	Z (normalized)
276.285	0.11434
459.256	0.19553
641.508	0.25818
821.963	0.32373
1001.990	0.37207
1180.038	0.42379
1355.664	0.49233
1531.384	0.53484
1705.924	0.56409
1876.676	0.65875

Table 9.7

Theoretical Values of Equivalent Circuit Parameters for Obstacle Width d= 1.62 mm

(Stycast line, ε_r= 10.6, w/h= 2.7, h= 5 mm, Z_0= 27 ohms)

Frequency (MHz)	Z (normalized)		
	$K_e = A_0$	$K_e = A_0 + A_1 \cos\frac{\pi u}{d}$	$K_e = A_0 + A_1 \cos\frac{\pi u}{d} + A_2 \cos\frac{2\pi u}{d}$
193.331	0.09978	0.09115	0.09070
386.523	0.19981	0.18257	0.18166
575.756	0.30039	0.27451	0.27315
762.799	0.40179	0.36726	0.36544
947.170	0.50432	0.46112	0.45885
1129.500	0.60832	0.55641	0.55368
1309.884	0.71418	0.65632	0.65033
1488.480	0.82231	0.75287	0.74921
1664.636	0.93324	0.85495	0.85082
1839.920	1.04757	0.96037	0.95578

Table 9.8

Theoretical Values of Equivalent Circuit Parameters for Obstacle Width d= 3.07 mm

(Stycast line, ε_r= 10.6, w/h=2.7, h= 5 mm, Z_0= 27 ohms)

Frequency (MHz)	Z (normalized)		
	$K_e = A_0$	$K_e = A_0 + A_1 \cos\frac{\pi u}{d}$	$K_e = A_0 + A_1 \cos\frac{\pi u}{d} + A_2 \cos\frac{2\pi u}{d}$
193.331	0.07274	0.06934	0.06818
386.523	0.14571	0.13892	0.13660
575.756	0.21919	0.20898	0.20550
762.799	0.29344	0.27978	0.27513
947.170	0.36874	0.35160	0.34579
1129.500	0.44543	0.42474	0.41775
1309.884	0.52384	0.49955	0.49138
1488.480	0.60439	0.57642	0.56706
1664.636	0.68756	0.65581	0.64526
1839.920	0.77394	0.73828	0.72652

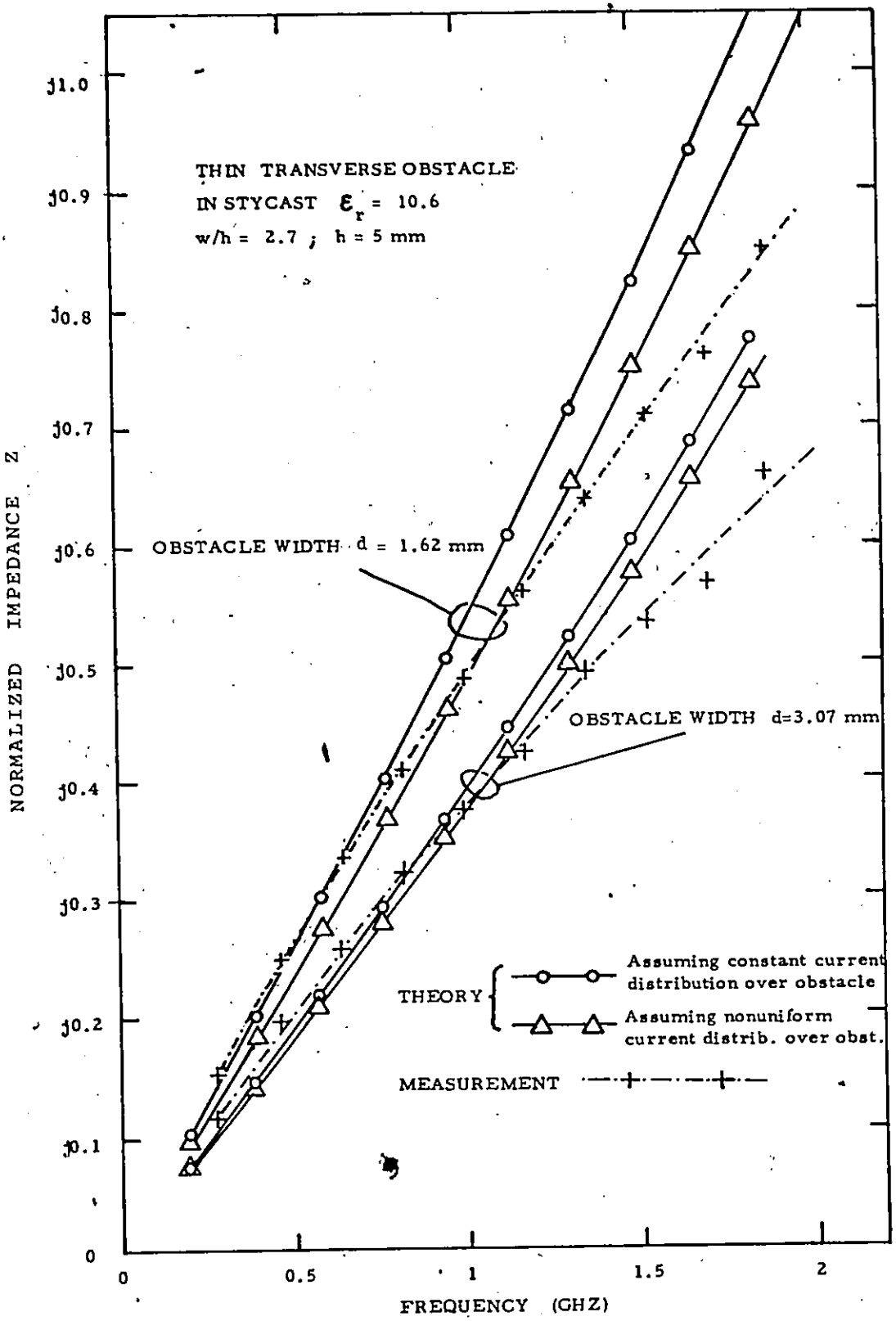

Figure 9.2 Normalized impedance of thin transverse obstacle in a 27Ω line on Stycast (ε_r=10.6; h=5 mm; w/h=2.7). Obstacle width d=1.62 mm; obstacle width d=3.07 mm.

These two sets of values differ more in the higher frequency range. The difference between theoretical and experimental results may be due to the following reason.

In the theoretical calculations, the microstrip was replaced by an ideal parallel plate model with magnetic sidewalls. Even though the radiation losses appear to be very small, the fringing effects cause a part of the radiation impedance to be reactive. The idealized model does not account for this fringing effect. It is the reactive part of the radiation impedance that affects the energy stored at the discontinuity.

It can be shown that (see chapter 10) the presence of the capacitive launcher does not have any effect on the final determination of the Z-parameters, so long as the frequency measurements before and after the introduction of the discontinuity are made with the same gap width between the launcher and the ring. However for the sake of interest, we have described in Appendix C, how the effect of the launcher can be eliminated from the frequency measurements themselves.

9.2 Centered Metallic Posts of Circular Cross-section

In the case of centered metallic posts of circular cross-section, unlike that for thin transverse obstacles, Z_{11} is not equal to Z_{12}. Hence for such obstacles, to obtain the impedance parameters, both even and odd excitations are to be investigated.

We have experimentally determined (in the range .1 - 2GHz) the equivalent Z-parameters of two centered metallic obstacles of circular cross-section having diameter d = 1/16 inch and d = 3/16 inch. As the first step, the resonance frequencies of the empty ring resonator (length = 59.124 cm) were determined. From these measurements, the corresponding dielectric constants of the substrate were calculated following the procedure shown in section 9.1. The effective dielectric constants at the different resonance frequencies of the ring are given in Table 9.9. This data has been plotted in Figure 9.3.

Table 9.9

ε_{eff} at the Resonante Frequencies of the Empty Ring

(Stycast line, ε_r = 10.6, w/h= 2.7, h= 5 mm, Z_0 = 27 ohms, ℓ_{ring} = 59.124 cm)

Harmonic No. n	Resonance Frequency (f_r) (MHz)	λ_t (cm)	ε_{eff}
1	187.800	59.124	7.28992
2	375.452	29.562	7.29216
3	559.389	19.708	7.39483
4	741.100	14.781	7.48997
5	920.433	11.825	7.58699
6	1097.923	9.854	7.67843
7	1273.137	8.446	7.77248
8	1446.759	7.391	7.86143
9	1619.082	6.569	7.94440
10	1789.288	5.912	8.03070
11	1958.268	5.375	8.11251
12	2125.752	4.927	8.19316

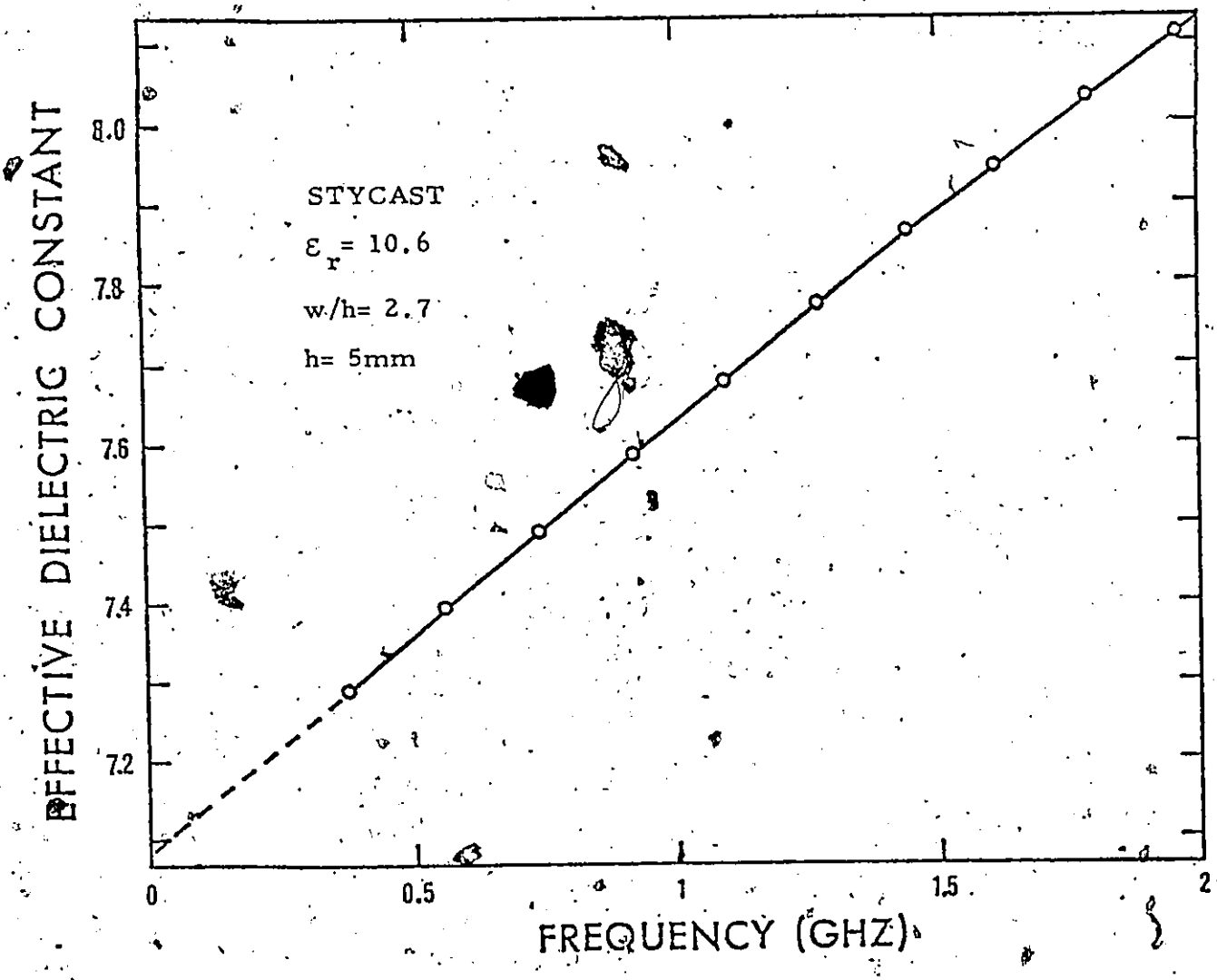

Figure 9.3 Measured effective dielectric constant for the microstrip ring. (ℓ_{ring} = 59.124 cm)

After the determination of ε_{eff} from the empty ring resonance measurements, two circular cylindrical centered metallic posts (diameter = 1/16 inch and 3/16 inch) were introduced into the ring one by one. The obstacles were realized, as has been described earlier, by drilling a centered hole across the ring and filling it with mercury. For each obstacle introduced, the corresponding sets of even and odd resonance frequencies were measured. For each of these frequencies, the corresponding ε_{eff} was determined using Table 9.9 following linear interpolation as described in section 9.1.

Once the even and odd resonance frequencies are known and the corresponding dielectric constants are determined, the even and odd input impedances of the equivalent circuit of the obstacle can be found using equations (7.1.9) and (7.1.10) respectively. The resonance frequencies, corresponding ε_{eff} values and the impedance values are given for two different posts in Tables 9.10, 9.11, 9.12 and 9.13.

The normalized even and odd impedances for the same two centered circular cylindrical metallic posts have been calculated theoretically using equations (5.1.20) and (5.2.8). These theoretical values for $Z_{11} + Z_{12}$ and $Z_{11} - Z_{12}$ are obtained for the empty resonance frequencies of the ring. The theoretical results are given in Tables 9.14 and 9.15.

The experimental and theoretical values of even impedance are compared in Figure 9.4 and those of odd impedance in Figure 9.5.

The measured values for the even impedances form a smooth curve while the values measured for the odd impedance are more scattered. This confirms the observation made in Chapter 10: the more the impedances differ from $\pm$ j1, the more sensitive they are to errors in frequency measurements.

The theoretical and experimental values are quite close in the lower frequency range. Towards higher frequencies, they differ more. The difference between the theoretical and experimental results can be explained, as was done in sections 4.3 and 9.1, by the fact that (1) only a

Table 9.10

Experimental Values of Even Resonance Frequencies, ε_{eff} and Normalized Even Input Impedance for Post Diameter= 1/16 inch

(Stycast line, ε_r= 10.6, w/h= 2.7, h= 5 mm, Z_0= 27 ohms, ℓ_{ring}=59.124 cm)

Even Resonance Frequency (MHz)	ε_{eff}	Norm. Even Input Impedance $Z_{11}+Z_{12}$
269.105	7.23272	2.32444×10^{-1}
448.096	7.33268	3.49357×10^{-1}
625.723	7.42956	4.56751×10^{-1}
801.614	7.52271	5.65976×10^{-1}
976.368	7.61580	6.61775×10^{-1}
1149.872	7.70631	7.49387×10^{-1}
1321.341	7.79718	8.45592×10^{-1}
1492.301	7.88336	9.19568×10^{-1}
1661.617	7.96597	1.00651
1829.568	8.05020	1.08163
1996.231	8.13079	1.16437

Table 9.11

Experimental Values of Odd Resonance Frequencies, ε_{eff} and Normalized Odd Input Impedance for Post Diameter = 1/16 inch

(Stycast line, $\varepsilon_r = 10.6$, w/h= 2.7, h= 5 mm, $Z_0 = 27$ ohms, $\ell_{ring} = 59.124$ cm)

Odd Resonance Frequency (MHz)	ε_{eff}	Norm. Odd Input Impedance $Z_{11} - Z_{12}$
374.918	7.29182	1.05938×10^{-2}
559.664	7.39498	-4.72779×10^{-3}
741.424	7.49014	-5.63629×10^{-3}
921.414	7.58752	-1.72897×10^{-2}
1098.788	7.67887	-1.53922×10^{-2}
1274.025	7.77296	-1.60148×10^{-2}
1447.801	7.86196	-1.89575×10^{-2}
1619.777	7.94475	-1.27649×10^{-2}
1790.201	8.03114	-1.68968×10^{-2}
1958.732	8.11273	-8.66697×10^{-3}

Table 9.12

Experimental Values of Even Resonance Frequencies, ε_{eff} and Normalized Even Input Impedance for Post Diameter = 3/16 inch

(Stycast line, $\varepsilon_r = 10.6$, w/h= 2.7, h= 5 mm, $Z_0 = 27$ ohms, $\ell_{ring} = 59.124$ cm)

Even Resonance Frequency (MHz)	ε_{eff}	Norm. Even Input Impedance $Z_{11} + Z_{12}$
276.876	7.23706	0.97838×10^{-1}
460.010	7.33933	1.33500×10^{-1}
641.231	7.43768	1.62042×10^{-1}
820.086	7.53270	1.94261×10^{-1}
997.153	7.62651	2.20732×10^{-1}
1172.634	7.71853	2.40091×10^{-1}
1345.842	7.80973	2.65286×10^{-1}
1517.787	7.89563	2.87149×10^{-1}
1688.429	7.97956	3.03430×10^{-1}
1856.863	8.06341	3.29162×10^{-1}
2024.136	8.14422	3.52235×10^{-1}

Table 9.13

Experimental Values of Odd Resonance Frequencies, ε_{eff} and Normalized Odd Input Impedance for Post Diameter = 3/16 inch

(Stycast line, ε_r = 10.6, w/h= 2.7, h= 5 mm, Z_0= 27 ohms, ℓ_{ring}= 59.124 cm)

Odd Resonance Frequency (MHz)	ε_{eff}	Norm. Odd Input Impedance $Z_{11} - Z_{12}$
375.737	7.29227	-3.30610×10^{-3}
560.777	7.39556	-2.38510×10^{-2}
743.025	7.49098	-3.35012×10^{-2}
923.308	7.58847	-5.06420×10^{-2}
1101.084	7.68012	-5.64100×10^{-2}
1276.773	7.77434	-6.55420×10^{-2}
1451.132	7.86353	-7.95090×10^{-2}
1623.536	7.94666	-8.19840×10^{-2}
1794.703	8.03332	-1.00550×10^{-1}
1963.444	8.11500	-9.69650×10^{-2}

Table 9.14

Theoretical Values of Normalized Even and Odd Input Impedance for Post Diameter = 1/16 inch

(Stycast line, $\varepsilon_r = 10.6$, w/h= 2.7, h= 5 mm, $Z_0 = 27$ ohms)

Frequency (MHz)	$Z_{11} + Z_{12}$ (normalized)	$Z_{11} - Z_{12}$ (normalized)
187.800	0.13049	-0.00086
375.452	0.26147	-0.00173
559.389	0.39344	-0.00259
741.100	0.52692	-0.00346
920.433	0.66248	-0.00432
1097.923	0.80073	-0.00519
1273.137	0.94234	-0.00605
1446.759	1.08810	-0.00692
1619.082	1.23892	-0.00778
1789.288	1.39586	-0.00865

Table 9.15

Theoretical Values of Normalized Even and Odd Input Impedance for Post Diameter = 3/16 inch

(Stycast line, ε_r= 10.6, w/h= 2.7, h= 5 mm, Z_0= 27 ohms)

Frequency (MHz)	$Z_{11}+Z_{12}$ (normalized)	$Z_{11}-Z_{12}$ (normalized)
187.800	0.04007	-0.00778
375.452	0.08056	-0.01556
559.389	0.12190	-0.02335
741.100	0.16455	-0.03113
920.433	0.20899	-0.03819
1097.423	0.25576	-0.04669
1273.137	0.30548	-0.05447
1446.759	0.35886	-0.06226
1619.082	0.41672	-0.07004
1789.288	0.48009	-0.07782

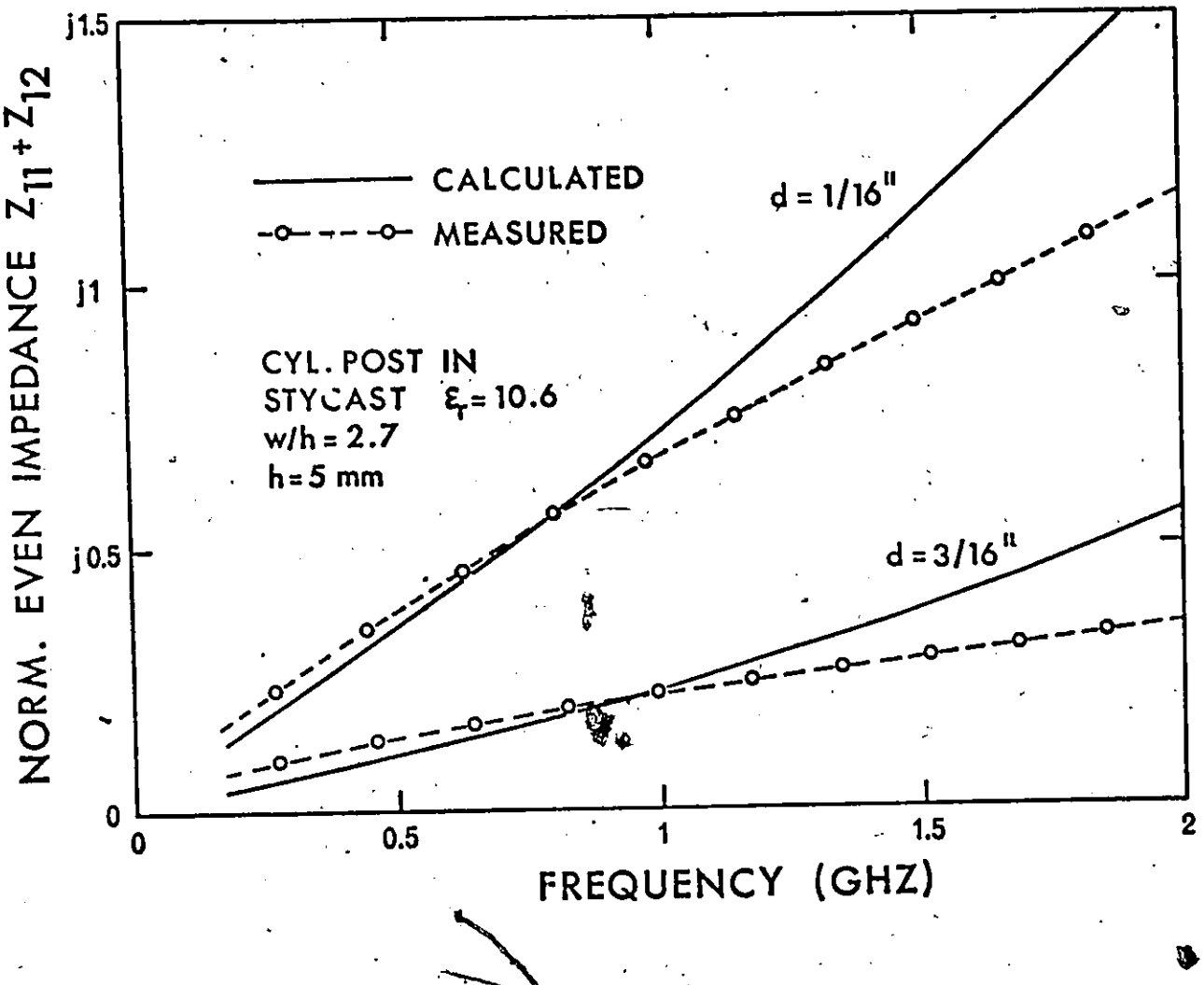

Figure 9.4 Normalized even impedances of centered metallic posts of circular cross-section in a 27Ω line on Stycast (ε_r=10.6; h=5 mm; w/h=2.7). Post diameter d=1/16 in., post diameter d=3/16 in.

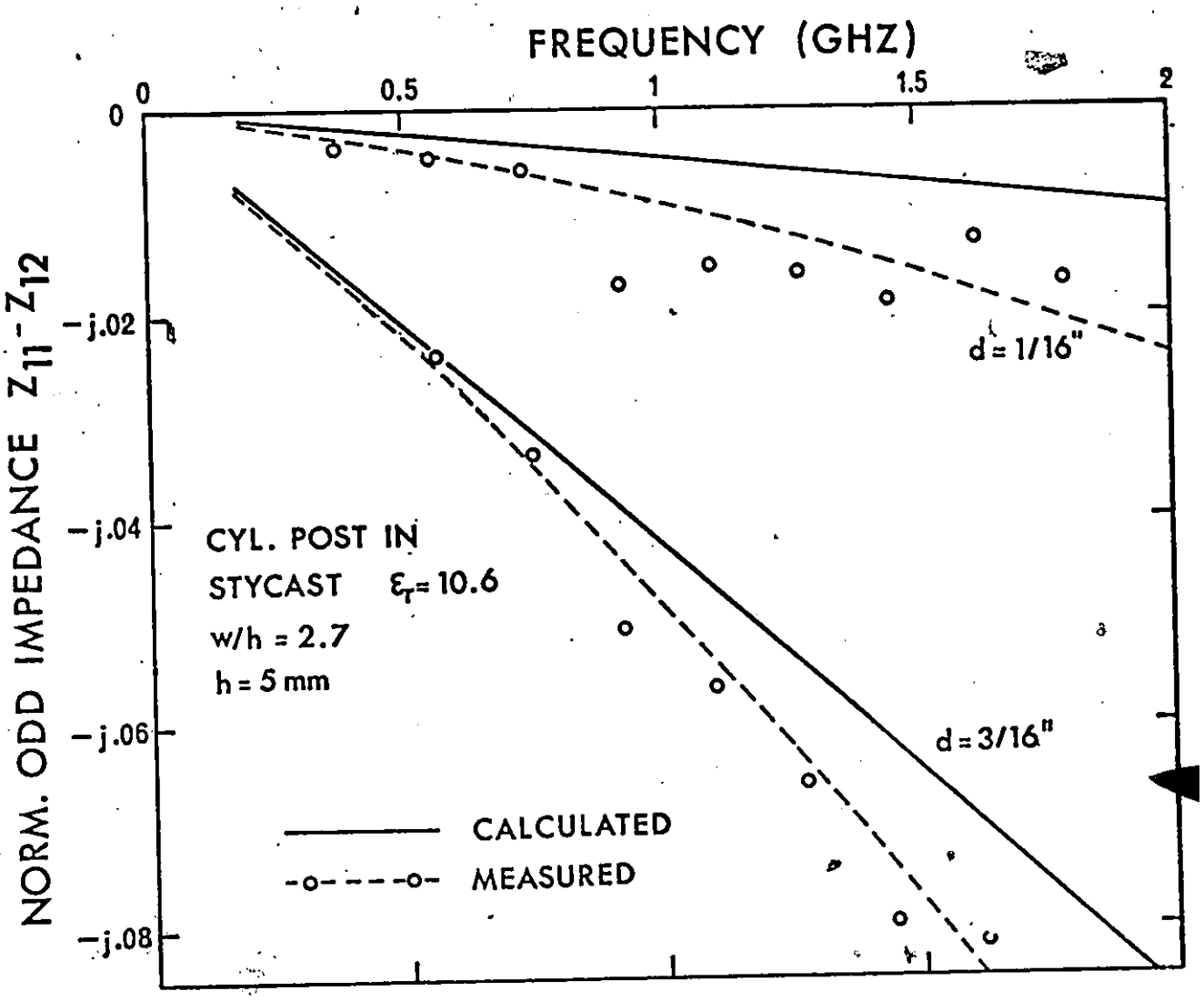

Figure 3.5 Normalized odd impedances of centered metallic posts of circular cross-section in a 27Ω line on Stycast (ε_r=10.6; h=5 mm; w/h=2.7). Post diameter d=1/16 in. post diameter d=3/16 in.

constant current distribution function was assumed and (2) the model used for the microstrip is only approximating the behaviour of the microstrip.

Let us now investigate the effect, on the theoretical evaluation of $Z_{11} + Z_{12}$, of the two following factors.

(a) Averaging the field over the crosssectional area of the cylindrical post, as suggested in section 5.3.

and (b) The summation term in the expression for $Z_{11} + Z_{12}$ as given by equation (5.1.20).

a. Instead of using equation (5.1.20) alone for the evaluation of even impedance of the cylindrical post, if we use the correction due to nonuniform field distribution as described in section 5.3, the relative change in the value of even impedance is not significant. It is evident from Tables 9.16 and 9.17 that over the whole frequency range, the effect of averaging of field over the post crosssection does not alter the values of even impedance by a significant amount. So, it is not necessary to consider the correction due to nonuniform field distribution for the even impedance evaluation.

b. The calculation of the summation term is the most cumbersome part of evaluating even impedance using equation (5.1.20). This term is always positive over the whole frequency range. It can be observed from Tables 9.16 and 9.17 and Figure 9.6 that by neglecting the summation term, the resulting relative change in the value of even impedance is negative and small for the lower frequencies but appreciable for the higher frequencies. So it, for the sake of convenience, we neglect the summation term. Although the dispersion of the TEM-mode is taken into account [λ_t in the formulae for discontinuities (5.1.20), (5.2.8)], dispersion for higher modes has not been considered. But this does not seem to be an important omission because neglecting of the higher order terms did not significantly improve the agreement between theoretical and experimental values.

Table 9.16

Comparison of the effect of the summation term (in the expression for even impedance) and the averaging of the field over circular cross-section on the even impedance of cylindrical posts

Post Diameter = 1/16 inch

(Stycast line, ε_r = 10.6, w/h= 2.7, h= 5 mm, Z_0= 27 ohms)

Frequency (MHz)	Normalized Even Impedance (Theory) $Z_{11}+ Z_{12}$	Relative Change in $Z_{11}+ Z_{12}$ after averaging of field over the post cross-section (%)	Relative Change in $Z_{11}+ Z_{12}$ when neglecting summation term (%)
187.800	0.13049	0	-0.070
375.452	0.26147	-0.008	-0.256
559.389	0.39344	-0.015	-0.574
741.100	0.52692	-0.028	-1.020
920.433	0.66248	-0.044	-1.605
1097.923	0.80073	-0.065	-2.322
1273.137	0.94234	-0.087	-3.183
1446.759	1.08810	-0.114	-4.236
1619.082	1.23892	-0.144	-5.336
1789.288	1.39586	-0.179	-6.820

Table 9.17

Comparison of the effect of the summation term (in the expression for even impedance) and the averaging of the field over circular cross-section on the even impedance of cylindrical posts

Post Diameter = 3/16 inch

(Stycast line , ε_r = 10.6, w/h= 2.7, h= 5 mm, Z_0= 27 ohms)

Frequency (MHz)	Normalized Even Impedance (Theory) $Z_{11}+Z_{12}$	Relative Change in $Z_{11}+Z_{12}$ after averaging of field over the post cross-section (%)	Relative Change in $Z_{11}+Z_{12}$ when neglecting summation term (%)
187.800	0.04007	0	- 0.225
375.452	0.08056	-0.062	- 0.832
559.389	0.12190	-0.139	- 1.857
741.100	0.16455	-0.255	- 3.156
920.433	0.20899	-0.402	- 5.089
1097.923	0.25576	-0.575	- 7.271
1273.137	0.30548	-0.782	- 9.878
1446.759	0.35886	-1.020	-12.711
1619.082	0.41672	-1.290	-15.902
1789.288	0.48009	-1.570	-19.424

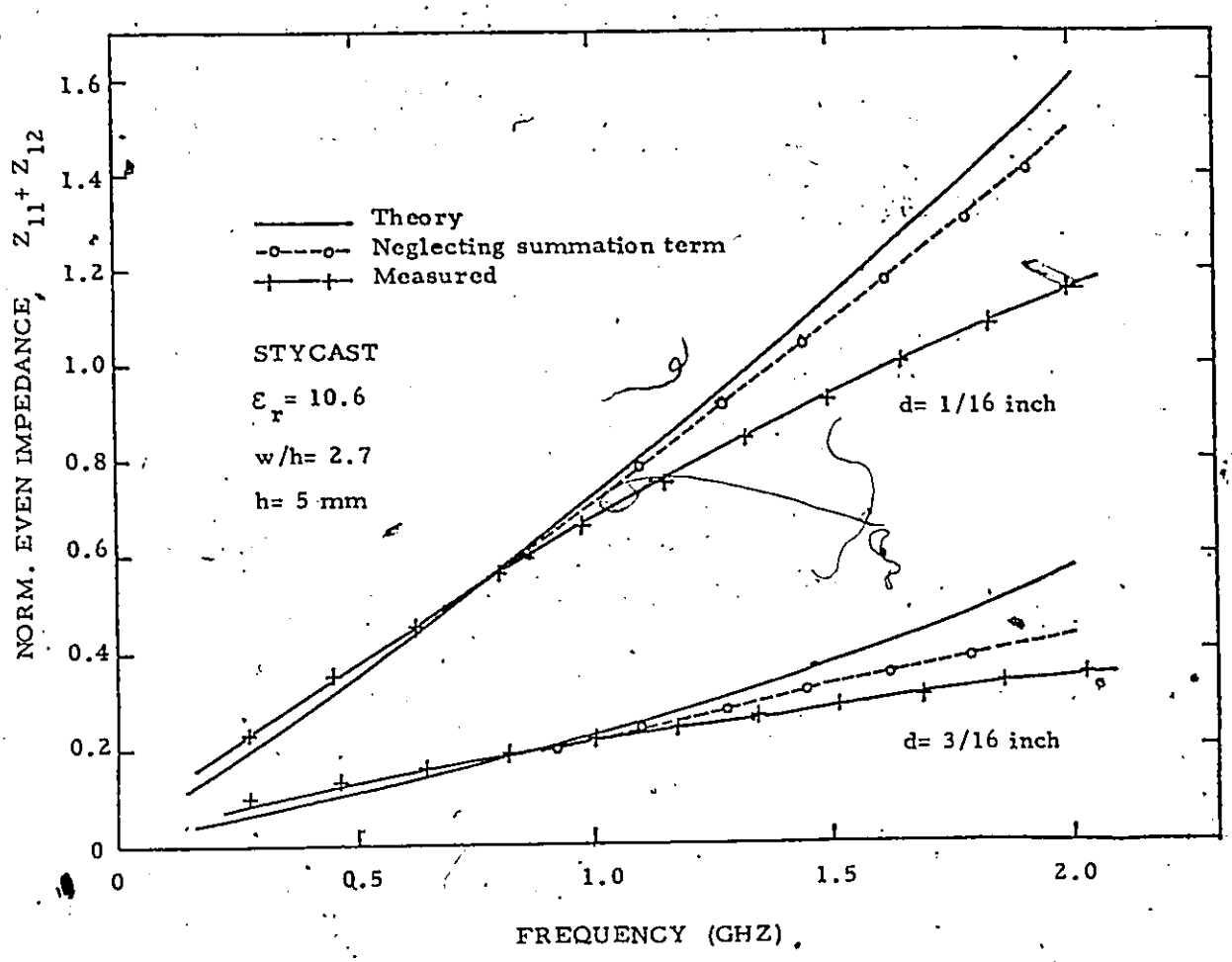

Figure 9.6 Comparison of the effect of the summation term (in the expression for even impedance) on the even impedance of cylindrical metallic posts of circular cross-section. Post diameter d= 1/16 inch , d= 3/16 inch.

CHAPTER 10

Error Analysis for Experimental Characterization of Lossless Discontinuities in Resonant Rings

A general study of the resonant ring method for the characterization of microstrip discontinuities have been given in Chapter 7. In the present chapter we will analyze the accuracy with which the equivalent circuit parameters of reciprocal lossless discontinuities can be measured in resonant rings [17].

Let us recall from Chapter 7 (equations (7.1.9) and (7.1.10)) that the normalized even and odd mode input impedances at either port of the equivalent circuit of Figure 3.2 can be given as

$$Z_{ie} = Z_{11} + Z_{12} = j \cot \left(\frac{\pi \ell_{ring} \sqrt{\varepsilon_{eff}(f_{re})}\, f_{re}}{c} \right) \qquad (10.1.1)$$

$$Z_{io} = Z_{11} - Z_{12} = -j \tan \left(\frac{\pi \ell_{ring} \sqrt{\varepsilon_{eff}(f_{ro})}\, f_{ro}}{c} \right) \qquad (10.1.2)$$

where ℓ_{ring} is the physical mean length of the ring, ε_{eff} is the effective dispersive dielectric constant of the line at the resonance frequencies of the loaded ring for even (f_{re}) and odd (f_{ro}) excitation of the discontinuity, and c is the velocity of light.

Moreover, as has been seen in Chapter 8, the measurement of the parameters of a lossless discontinuity is performed in two stages:

i) The resonant frequencies of the ring are measured before the discontinuity is introduced. They yield the dispersive permittivity ε_{eff} of the line.

ii) The discontinuity is then introduced and the degenerated even and odd resonance frequencies of the structure are measured. Since these frequencies are in general different from those

measured in i), the values of ε_{eff} that are used in equations (10.1.1) and (10.1.2) must be found by interpolation.

When the systematic errors due to dimensional inaccuracies of the resonant ring are practically eliminated, the accuracy of the measured discontinuity impedances depends on the accuracy with which the frequency of the resonance peaks can be located and measured.

Let us first consider how the even discontinuity impedance Z_{ie} is susceptible to the errors in frequency measurements. Since the error in the measurement of Z_{ie} depends on the error with which both empty and loaded ring resonance frequencies are determined, we can write

$$dZ_{ie} = \frac{\partial Z_{ie}}{\partial f_e} df_e + \frac{\partial Z_{ie}}{\partial f_{re}} df_{re} \qquad (10.1.3)$$

where f_e denotes the resonance frequency of the empty ring. We shall evaluate the two terms of equation (10.1.3) separately.

Z_{ie} is dependent on the empty resonance frequency implicitly through ε_{eff}. So, we can write

$$\frac{\partial Z_{ie}}{\partial f_e} = \frac{\partial Z_{ie}}{\partial(\sqrt{\varepsilon_{eff}})} \cdot \frac{\partial(\sqrt{\varepsilon_{eff}})}{\partial f_e} \qquad (10.1.4)$$

Using equation (10.1.1),

$$\frac{\partial Z_{ie}}{\partial(\sqrt{\varepsilon_{eff}})} = -j \frac{\pi \ell_{ring} f_{re}}{c} \cdot \frac{1}{\sin^2\left(\frac{\pi \ell_{ring} \sqrt{\varepsilon_{eff}}\, f_{re}}{c}\right)} \qquad (10.1.5)$$

Now,

$$\frac{1}{\sin^2\left(\frac{\pi \ell_{ring} \sqrt{\varepsilon_{eff}}\, f_{re}}{c}\right)} = 1 + \cot^2\left(\frac{\pi \ell_{ring} \sqrt{\varepsilon_{eff}}\, f_{re}}{c}\right) \qquad (10.1.6)$$

$$= 1 + Z_{ie} Z_{ie}^{*} \quad \text{(by equation (10.1.1))} \qquad (10.1.7)$$

$$= 1 + |Z_{ie}|^2 \qquad (10.1.8)$$

Therefore,

$$\frac{\partial Z_{ie}}{\partial(\sqrt{\varepsilon_{eff}})} = -j\ (1 + |Z_{ie}|^2)\ \frac{\pi \ell_{ring} f_{re}}{c} \qquad (10.1.9)$$

Again,

$$\frac{\partial(\sqrt{\varepsilon_{eff}})}{\partial f_e} = -\frac{nc}{\ell_{ring}} \cdot \frac{1}{f_e^2} \left[\because \sqrt{\varepsilon_{eff}} = \frac{nc}{\ell_{ring} f_e} \right] \qquad (10.1.10)$$

$$= -\frac{\sqrt{\varepsilon_{eff}}}{f_e} \qquad (10.1.11)$$

So, using equations (10.1.4), (10.1.9) and (10.1.11),

$$\frac{\partial Z_{ie}}{\partial f_e} = j\ (1+ |Z_{ie}|^2)\ \frac{\pi \ell_{ring} \sqrt{\varepsilon_{eff}}}{c} \cdot \frac{f_{re}}{f_e} \qquad (10.1.12)$$

Now, let us see the dependence of Z_{ie} on f_{re}. In equation (10.1.1) f_{re} appears both explicitly and implicitly (due to the presence of ε_{eff}). Since ε_{eff} increases linearly with frequency, we may write

$$\varepsilon_{eff}(f_{re}) = \varepsilon_1 + b f_{re} \qquad (10.1.13)$$

where ε_1 = effective permittivity at zero frequency

and $b = d\varepsilon_{eff}/df$ = slope of ε_{eff} vs frequency plot.

Using this we obtain,

$$\frac{\partial Z_{ie}}{\partial f_{re}} = -j(1 + |Z_{ie}|^2) \frac{\pi \ell_{ring}}{c} \left[\frac{b f_{re}}{2\sqrt{\varepsilon_1 + b f_{re}}} + \sqrt{\varepsilon_1 + b f_{re}} \right] \qquad (10.1.14)$$

$$= -j(1 + |Z_{ie}|^2) \frac{\pi \ell_{ring}}{c} \left[\frac{3\varepsilon_{eff} - \varepsilon_1}{2\sqrt{\varepsilon_{eff}}} \right] \qquad (10.1.15)$$

Hence combining equations (10.1.3), (10.1.12) and (10.1.15) we get,

$$\frac{dZ_{ie}}{Z_{ie}} = j \frac{(1+|Z_{ie}|^2)}{Z_{ie}} \cdot \frac{\pi \ell_{ring}}{c} \cdot \left[\sqrt{\varepsilon_{eff}} \frac{f_{re}}{f_e} df_e + \frac{\varepsilon_1 - 3\varepsilon_{eff}}{2\sqrt{\varepsilon_{eff}}} df_{re}\right] \quad (10.1.16)$$

Proceeding in a similar way for Z_{io} we get exactly the same expression for dZ_{io}/Z_{io}.

Under the conditions that

(a) even and odd resonance frequencies are very close to empty resonance frequencies.

and (b) $bf/\varepsilon_1 << 1$ (where f = either f_{re} or f_{ro}),

both of which hold in practice, the expression for the relative error in the measurement of even as well as odd discontinuity impedance simplifies to

$$\frac{dZ_i}{Z_i} = j \frac{(1 + |Z_i|^2)}{Z_i} \cdot \frac{\pi \ell_{ring} \sqrt{\varepsilon_{eff}}}{c} (df_e - df_r) \quad (10.1.17)$$

where df_e and df_r denote the absolute errors committed in the measurement of empty and loaded ring frequencies respectively. These errors reflect the precision with which the resonance frequencies of the ring can be located. It is not so much determined by the accuracy of the frequency counter as by the sharpness of the observed resonance peaks. A good estimate of df_e and df_r can be obtained by measuring several times the resonance frequencies and finding the standard deviation of the results from their calculated average.

Table 10.1 presents the relative error in discontinuity impedance as a function of absolute impedance values for several standard deviations for the worst case where $df_e = -df_r$. The same results are presented graphically in Figure 10.1.

From equation (10.1.17) and Figure 10.1 we can conclude the following :

Table 10.1

Relative Error in (Normalized) Discontitinuity Impedance as a Function of Absolute (Normalized) Impedance

(Stycast line, ℓ_{ring} =59.124 cm, ε_{eff} = 7.60)

Z_i (normalized)	dZ_i/Z_i (normalized) in % for $df_e = - df_r$ =			
	30 KHz	40 KHz	50 KHz	60 KHz
1	0.205	0.273	0.342	0.410
0.1	1.035	1.380	1.725	2.070
0.01	10.249	13.666	17.082	20.499
0.001	102.483	136.644	170.805	204.966

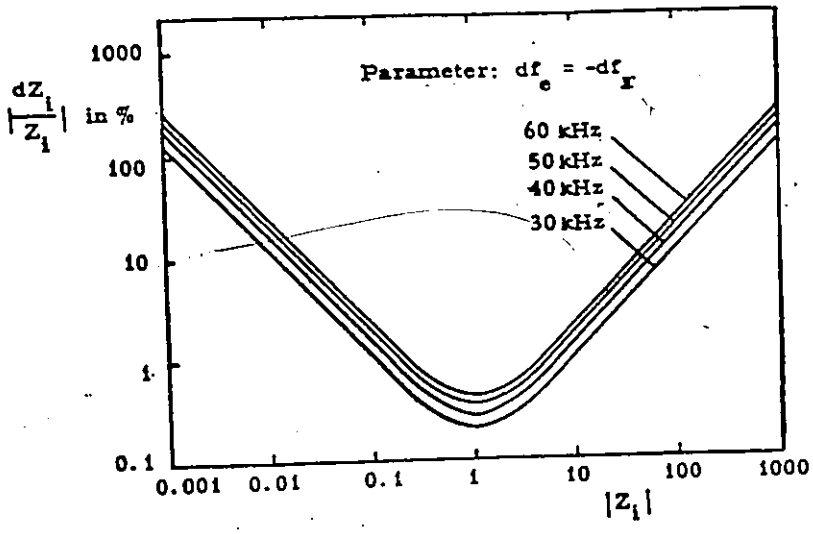

Figure 10.1 Relative error in discontinuity impedance vs. absolute impedance for several values of resolution in frequency measurements. ($\varepsilon_{eff} = 7.6$, $\ell_{ring} = 59.124$ cm)

1) The accuracy of the discontinuity impedance values is directly proportional to the accuracy with which the resonance frequencies can be located and measured.

2) For a given accuracy in frequency measurements, the obtained impedance value is most accurate if the absolute value of the normalized impedance is close to unity.

3) All errors affecting the measurement of f_e and f_r in the same way have practically no effect on the accuracy of Z_i. Thus the influence of the capacitive launcher on the measurement of the discontinuity impedances can be neglected as long as the coupling gap is the same for all measurements.

CHAPTER 11

Conclusions

In the present work, both theoretical and experimental determination of discontinuity parameters in microstrip lines have been studied. For both the approaches, a general method of characterization has been developed and then demonstrated with the aid of some specific examples.

For the theoretical determination, as opposed to static approximations, a dynamic approach was adopted. A general discontinuity was represented by an equivalent T-circuit in the Wheeler's idealized parallel plate model with magnetic sidewalls. The model describes accurately the TEM-mode propagation and approximates the higher order modes. The even and odd mode input impedance of the T-equivalent was represented by a variational expression that contains a dynamic Green's function and approximate current distribution function over the obstacle surface. The current distribution is approximated by a Fourier series. Numerical evaluation of impedance parameters have been made for thin metallic plates and circular cylindrical metallic posts in the quasi-TEM range. The results are in very good agreement with experimental values for the lower frequencies, though they tend to be less accurate for higher frequencies. It has been shown that the consideration of more than two terms of the Fourier expansion of current distribution on the obstacle surface does not appreciably increase the accuracy of the theoretical results. The difference between the theoretical and experimental values can be explained by the inadequacy of the parallel plate model for the microstrip at high frequencies.

For experimental characterization of discontinuities in microstrip circuits, the resonant ring method has been in use for some time. This method has the advantage of eliminating the effect of coaxial-to-microstrip transitions. Until now the resonant ring method has been used only for

particular types of discontinuities. In the present work, a comprehensive analysis for a general discontinuity in a resonant ring has been made. This enables the method to be applied to a large variety of discontinuities. The experimental technique to determine the equivalent T-circuit reactances of a discontinuity is very simple and convenient, consisting of only the determination of resonant frequencies of the ring resonator. The method has been used to study the parameters of thin metallic plates and circular cylindrical posts. Very good results are obtained by this approach where the value of the normalized reactance of a discontinuity is between $\pm$ j 100 and $\pm$ j0.01. Evaluation of the losses is more difficult, since this involves measurement of changes in Q-factor, a procedure inherently less accurate than the measurement of resonant frequencies.

It is believed that the resonant ring method described in the thesis is the most accurate method available to date for experimental characterization of microstrip discontinuities. It is particularly suited for verifying results obtained by any analytical or numerical method.

APPENDIX A

Calculation of D_{mn}'s

We know from equation (3.2.23), $(z = z' \neq 0)$

$$G'(u, z; u', z') = \frac{j}{A} \sum_{m=1}^{\text{odd } m} \frac{1}{k_m} \sin \frac{m\pi u}{A} \sin \frac{m\pi u'}{A} + \frac{j}{A} \sum_{m=2}^{\text{even } m} \frac{1}{k_m} \cos \frac{m\pi u}{A} \cos \frac{m\pi u'}{A} \qquad (A1)$$

and from equation (3.3.3),

$$D_{mn} = \int_{\text{obstacle}} \int f_n(u, z)\, G'(u, z; u', z')\, f_m(u', z')\, dS\, dS' \qquad (A2)$$

With the help of (A1) and (A2) we can proceed to calculate the D_{mn}'s as follows.

I. D_{11}

$$D_{11} = \int_{\text{obs.}} \int_{\text{obs.}} G'(u, z; u', z')\, dS\, dS' \qquad (A3)$$

a. Calculation with the first (summation) term of G'.

Consider the m^{th} term.

$$\frac{j}{A} \cdot \frac{1}{k_m} \int_{\text{obs}} \int_{\text{obs}} \sin \frac{m\pi u}{A} \sin \frac{m\pi u'}{A}\, du\, du' \qquad (A4)$$

$$= \frac{j}{A} \cdot \frac{1}{k_m} \left[\int_{-d/2}^{d/2} \sin \frac{m\pi u}{A}\, du + \int_{d/2}^{-d/2} \sin \frac{m\pi u}{A} (-du) \right]$$

$$\times \left[\int_{-d/2}^{d/2} \sin \frac{m\pi u'}{A}\, du' + \int_{d/2}^{-d/2} \sin \frac{m\pi u'}{A} (-du') \right] \qquad (A5)$$

$$= \frac{j}{A} \cdot \frac{4}{k_m} \int_{-d/2}^{d/2} \sin \frac{m\pi u}{A}\, du \int_{-d/2}^{d/2} \sin \frac{m\pi u'}{A}\, du' \qquad (A6)$$

$= 0$, since sine is an even function and we are integrating from $-d/2$ to $d/2$. (A7)

So, there is no contribution to D_{11} due to the first (summation) term of G'.

b. Calculation with the second (summation) term of G'.

Consider the m^{th} term.

$$\frac{j}{A} \cdot \frac{1}{k_m} \int_{obs} \int_{obs} \cos \frac{m\pi u}{A} \cos \frac{m\pi u'}{A} \, du \, du' \quad (A8)$$

$$= \frac{j}{A} \cdot \frac{4}{k_m} \int_{-d/2}^{d/2} \cos \frac{m\pi u}{A} \, du \int_{-d/2}^{d/2} \cos \frac{m\pi u'}{A} \, du' \quad [\text{as in (A6)}] \quad (A9)$$

$$= \frac{j}{A} \cdot \frac{4}{k_m} \cdot \left[\frac{A}{m\pi} \cdot 2 \sin \frac{m\pi d}{2A}\right] \left[\frac{A}{m\pi} \cdot 2 \sin \frac{m\pi d}{2A}\right] \quad (A10)$$

$$= j \frac{16A}{k_m m^2 \pi^2} \sin^2 \frac{m\pi d}{2A} \quad (A11)$$

Hence, we have using (A1), (A3) and (A11)

$$D_{11} = \sum_{m=2}^{even} j \frac{16A}{k_m m^2 \pi^2} \sin^2 \frac{m\pi d}{2A} \quad (A12)$$

II. D_{22}

$$D_{22} = \int_{obs} \int_{obs} \cos \frac{\pi u}{d} \, G'(u, z; u', z') \cos \frac{\pi u'}{d} \, du \, du' \quad (A13)$$

a. Calculation with the first (summation) term of G'.

Consider the m^{th} term.

$$\frac{j}{A} \cdot \frac{1}{k_m} \int_{obs} \int_{obs} \cos \frac{\pi u}{d} \sin \frac{m\pi u}{A} \sin \frac{m\pi u'}{A} \cos \frac{\pi u'}{d} \, du \, du' \quad (A14)$$

$$= \frac{j}{A} \cdot \frac{4}{k_m} \int_{-d/2}^{d/2} \cos\frac{\pi u}{d} \sin\frac{m\pi u}{A}\, du \int_{-d/2}^{d/2} \cos\frac{\pi u'}{d} \sin\frac{m\pi u'}{A}\, du'$$

[as in (A6)] (A15)

Now, $\int_{-d/2}^{d/2} \cos\frac{\pi u}{d} \cdot \sin\frac{m\pi u}{A}\, du$

$$= \frac{1}{2} \int_{-d/2}^{d/2} \sin\left(\frac{m\pi}{A} + \frac{\pi}{d}\right)u\, du + \frac{1}{2} \int_{-d/2}^{d/2} \sin\left(\frac{m\pi}{A} - \frac{\pi}{d}\right)u\, du \qquad (A16)$$

$$= 0. \quad [\text{as in (A7)}] \qquad (A17)$$

So, there is no contribution to D_{22} due to the first (summation) term of G'.

b. Calculation with the second (summation) term of G'.

Consider the m^{th} term.

$$\frac{j}{A} \frac{1}{k_m} \int_{obs} \int_{obs} \cos\frac{\pi u}{d} \cos\frac{m\pi u}{A} \cos\frac{m\pi u'}{A} \cos\frac{\pi u'}{d}\, du\, du' \qquad (A18)$$

$$= \frac{j}{A} \frac{4}{k_m} \int_{-d/2}^{d/2} \cos\frac{m\pi u}{A} \cos\frac{\pi u}{d}\, du \int_{-d/2}^{d/2} \cos\frac{m\pi u'}{A} \cos\frac{\pi u'}{d}\, du'$$

[as in (A6)] (A19)

Now, $\int_{-d/2}^{d/2} \cos\frac{m\pi u}{A} \cos\frac{\pi u}{d}\, du$

$$= \frac{1}{2} \int_{-d/2}^{d/2} \cos\left(\frac{m\pi}{A} + \frac{\pi}{d}\right)u\, du + \frac{1}{2} \int_{-d/2}^{d/2} \cos\left(\frac{m\pi}{A} - \frac{\pi}{d}\right)u\, du \qquad (A20)$$

$$= \frac{1}{2} \frac{1}{\left(\frac{m\pi}{A} + \frac{\pi}{d}\right)} \sin\left(\frac{m\pi}{A} + \frac{\pi}{d}\right)u\Big]_{-d/2}^{d/2} + \frac{1}{2} \frac{1}{\left(\frac{m\pi}{A} - \frac{\pi}{d}\right)} \sin\left(\frac{m\pi}{A} - \frac{\pi}{d}\right)u\Big]_{-d/2}^{d/2} \qquad (A21)$$

$$= \frac{2A^2 d}{\pi A^2 - m^2 \pi d^2} \cos\frac{m\pi d}{2A} \qquad (A22)$$

Hence, using (A1), (A13), (A19) and (A22) we have

$$D_{22} = \sum_{m=2}^{\text{even}} j \frac{16\, d^2}{A\, k_m\, \pi^2 (1 - m^2 \frac{d^2}{A^2})^2} \cos^2 \frac{m\pi d}{2A} \qquad \text{(A23)}$$

III. D_{33}

$$D_{33} = \int_{\text{obs}} \int_{\text{obs}} \cos \frac{2\pi u}{d}\, G'(u, z; u', z') \cos \frac{2\pi u'}{d}\, du\, du' \qquad \text{(A24)}$$

a. Calculation with the first (summation) term of G'.

Consider m^{th} term.

$$\frac{j}{A} \frac{1}{k_m} \int_{\text{obs}} \int_{\text{obs}} \cos \frac{2\pi u}{d} \sin \frac{m\pi u}{A} \sin \frac{m\pi u'}{A} \cos \frac{2\pi u'}{d}\, du\, du' \qquad \text{(A25)}$$

$$= \frac{j}{A} \frac{4}{k_m} \int_{-d/2}^{d/2} \sin \frac{m\pi u}{A} \cos \frac{2\pi u}{d}\, du \int_{-d/2}^{d/2} \sin \frac{m\pi u'}{A} \cos \frac{2\pi u'}{d}\, du'$$

[as in (A6)] (A26)

Now $$\int_{-d/2}^{d/2} \sin \frac{m\pi u}{A} \cos \frac{2\pi u}{d}\, du = 0 \quad \text{[as in (A17)]} \qquad \text{(A27)}$$

So, there is no contribution to D_{33} due to the first (summation) term of G'.

b. Calculation with the second (summation) term of G'.

Consider m^{th} term.

$$\frac{j}{A} \frac{1}{k_m} \int_{\text{obs}} \int_{\text{obs}} \cos \frac{2\pi u}{d} \cos \frac{m\pi u}{A} \cos \frac{m\pi u'}{A} \cos \frac{2\pi u'}{d}\, du\, du' \qquad \text{(A28)}$$

$$= \frac{j}{A} \frac{4}{k_m} \int_{-d/2}^{d/2} \cos \frac{m\pi u}{A} \cos \frac{2\pi u}{d}\, du \int_{-d/2}^{d/2} \cos \frac{m\pi u'}{A} \cos \frac{2\pi u'}{d}\, du'$$

[as in (A6)] (A29)

Now, $$\int_{-d/2}^{d/2} \cos \frac{m\pi u}{A} \cos \frac{2\pi u}{d} \, du$$

$$= \frac{1}{2} \int_{-d/2}^{d/2} \cos \left(\frac{m\pi}{A} + \frac{2\pi}{d}\right) u \, du + \frac{1}{2} \int_{-d/2}^{d/2} \cos \left(\frac{m\pi}{A} - \frac{2\pi}{d}\right) u \, du \qquad \text{(A30)}$$

$$= \frac{1}{2} \frac{1}{\left(\frac{m\pi}{A} + \frac{2\pi}{d}\right)} \sin \left(\frac{m\pi}{A} + \frac{2\pi}{d} \right) u \Big]_{-d/2}^{d/2} + \frac{1}{2} \frac{1}{\left(\frac{m\pi}{A} - \frac{2\pi}{d}\right)} \sin \left(\frac{m\pi}{A} - \frac{2\pi}{d}\right) u \Big]_{-d/2}^{d/2} \qquad \text{(A31)}$$

$$= \frac{2 m A d^2}{\pi (4A^2 - m^2 d^2)} \sin \frac{m\pi d}{2A} \qquad \text{(A32)}$$

Hence, using (A1), (A24), (A29) and (A32) we have

$$D_{33} = \sum_{m=2}^{\text{even}} j \frac{16 m^2 A}{k_m \pi^2 \left(4 \frac{A^2}{d^2} - m^2\right)^2} \sin^2 \frac{m\pi d}{2A} \qquad \text{(A33)}$$

IV. D_{12}, D_{21}

$$D_{12} \int_{\text{obs.}} \int_{\text{obs.}} G'(u, z ; u', z') \cos \frac{\pi u'}{d} \, du \, du' = D_{21} \qquad \text{(A34)}$$

a. Calculation with the first (summation) term of G'.

Consider the m^{th} term.

$$\frac{j}{A} \cdot \frac{1}{k_m} \int_{\text{obs.}} \int_{\text{obs.}} \sin \frac{m\pi u}{A} \sin \frac{m\pi u'}{A} \cos \frac{\pi u'}{d} \, du \, du' \qquad \text{(A35)}$$

$$= \frac{j}{A} \frac{4}{k_m} \int_{-d/2}^{d/2} \sin \frac{m\pi u}{A} \, du \int_{-d/2}^{d/2} \sin \frac{m\pi u'}{A} \cos \frac{\pi u'}{d} \, du'$$

[as in (A6)] (A36)

$$= 0 \quad \text{[as in (A7)]} \qquad \text{(A37)}$$

So, there is no contribution to D_{12} and D_{21} due to the first (summation) term of G'.

b. Calculation with the second (summation) term of G'.

Consider the m^{th} term.

$$\frac{j}{A}\frac{1}{k_m}\int_{obs.}\int_{obs.} \cos\frac{m\pi u}{A}\cos\frac{m\pi u'}{A}\cos\frac{\pi u'}{d}\,du\,du' \qquad (A38)$$

$$= \frac{j}{A}\frac{4}{k_m}\int_{-d/2}^{d/2}\cos\frac{m\pi u}{A}\,du\int_{-d/2}^{d/2}\cos\frac{m\pi u'}{A}\cos\frac{\pi u'}{d}\,du' \text{ [as in (A6)]} \qquad (A39)$$

Now, $$\int_{-d/2}^{d/2}\cos\frac{m\pi u}{A}\,du = \frac{A}{m\pi}\cdot 2\sin\frac{m\pi d}{2A} \quad \text{[as in (A10)]} \qquad (A40)$$

Again, $$\int_{-d/2}^{d/2}\cos\frac{m\pi u'}{A}\cos\frac{\pi u'}{d}\,du' = \frac{2A^2 d}{\pi A^2 - m^2\pi d^2}\cos\frac{m\pi d}{2A} \text{ [as in A22)]} \qquad (A41)$$

Hence, using (A1), (A34), (A39), (A40) and (A41) we have

$$D_{12} = D_{21} = \sum_{m=2}^{even} j\,\frac{8d}{mk_m\pi^2\left(1-m^2\frac{d^2}{A^2}\right)}\sin\frac{m\pi d}{A} \qquad (A42)$$

V D_{13}, D_{31}

$$D_{13} = \int_{obs}\int_{obs} G'(u,z;u',z')\cos\frac{2\pi u'}{d}\,du\,du' = D_{31} \qquad (A43)$$

a. Calculation with the first (summation) term of G'.

Consider the m^{th} term

$$\frac{j}{A}\frac{1}{k_m}\int_{obs}\int_{obs}\sin\frac{m\pi u}{A}\sin\frac{m\pi u'}{A}\cos\frac{2\pi u'}{d}\,du\,du' \qquad (A44)$$

$$= \frac{j}{A}\frac{4}{k_m}\int_{-d/2}^{d/2}\sin\frac{m\pi u}{A}\,du\int_{-d/2}^{d/2}\sin\frac{m\pi u'}{A}\cos\frac{2\pi u'}{d}\,du' \text{ [as in (A6)]} \qquad (A45)$$

$$= 0 \quad \text{[as in (A7)]} \qquad (A46)$$

So, there is no contribution to D_{13} and D_{31} due to the first (summation) term of G'.

b. Calculation with the second (summation) term of G'.

Consider the m^{th} term.

$$\frac{j}{A}\frac{1}{k_m}\int_{obs}\int_{obs} \cos\frac{m\pi u}{A}\cos\frac{m\pi u'}{A}\cos\frac{2\pi u'}{d}\,du\,du' \qquad (A47)$$

$$= \frac{j}{A}\frac{4}{k_m}\int_{-d/2}^{d/2}\cos\frac{m\pi u}{A}\,du\int_{-d/2}^{d/2}\cos\frac{m\pi u'}{A}\cos\frac{2\pi u'}{d}\,du' \quad [\text{as in (A6)}] \qquad (A48)$$

Now $$\int_{-d/2}^{d/2}\cos\frac{m\pi u}{A}\,du = \frac{A}{m\pi}\cdot 2\sin\frac{m\pi d}{2A} \quad [\text{as in (A10)}] \qquad (A49)$$

Again $$\int_{-d/2}^{d/2}\cos\frac{m\pi u'}{A}\cos\frac{2\pi u'}{d}\,du' = \frac{2mAd^2}{\pi(4A^2-m^2d^2)}\sin\frac{m\pi d}{2A} \quad [\text{as in (A32)}] \qquad (A50)$$

Hence, using (A1), (A43), (A48), (A49) and (A50) we have

$$D_{13} = D_{31} = \sum_{m=2}^{even} j\,\frac{16A}{k_m\pi^2(4\frac{A^2}{d^2}-m^2)}\sin^2\frac{m\pi d}{2A} \qquad (A51)$$

VI. D_{23}, D_{32}

$$D_{23} = \int_{obs}\int_{obs}\cos\frac{\pi u}{d}\,G'(u,z;u',z')\cos\frac{2\pi u'}{d}\,du\,du' = D_{32} \qquad (A52)$$

a. Calculation with the first (summation) term of G'.

Consider the m^{th} term.

$$\frac{j}{A}\frac{1}{k_m}\int_{obs}\int_{obs}\cos\frac{\pi u}{d}\sin\frac{m\pi u}{A}\sin\frac{m\pi u'}{A}\cos\frac{2\pi u'}{d}\,du\,du' \qquad (A53)$$

$$= \frac{j}{A}\frac{4}{k_m}\int_{-d/2}^{d/2}\sin\frac{m\pi u}{A}\cos\frac{\pi u}{d}\,du\int_{-d/2}^{d/2}\sin\frac{m\pi u'}{A}\cos\frac{2\pi u'}{d}\,du' \quad [\text{as in (A6)}] \qquad (A54)$$

$$= 0 \quad [\text{as in (A17)}] \qquad (A55)$$

So, there is no contribution to D_{23} and D_{32} due to the first (summation) term of G'.

b. Calculation with the second (summation) term of G'.

Consider the m^{th} term.

$$\frac{j}{A}\frac{1}{k_m}\int_{obs}\int_{obs}\cos\frac{\pi u}{d}\cos\frac{m\pi u}{A}\cos\frac{m\pi u'}{A}\cos\frac{2\pi u'}{d}\,du\,du' \qquad (A56)$$

$$= \frac{j}{A}\frac{4}{k_m}\int_{-d/2}^{d/2}\cos\frac{m\pi u}{A}\cos\frac{\pi u}{d}\,du\int_{-d/2}^{d/2}\cos\frac{m\pi u'}{A}\cos\frac{2\pi u'}{d}\,du' \quad [\text{as in (A6)}] \qquad (A57)$$

Now, $$\int_{-d/2}^{d/2}\cos\frac{m\pi u}{A}\cos\frac{\pi u}{d}\,du = \frac{2A^2 d}{\pi A^2 - m^2\pi d^2}\cos\frac{m\pi d}{2A} \quad [\text{as in (A22)}] \qquad (A58)$$

Again $$\int_{-d/2}^{d/2}\cos\frac{m\pi u'}{A}\cos\frac{2\pi u'}{d}\,du' = \frac{2mAd^2}{\pi(4A^2 - m^2d^2)}\sin\frac{m\pi d}{2A} \quad [\text{as in (A32)}] \qquad (A59)$$

Hence, using (A1), (A52), (A57), (A58) and (A59) we have

$$D_{23} = D_{32} = \sum_{m=2}^{\text{even}} j\,\frac{8md}{k_m\pi^2\left(1-m^2\frac{d^2}{A^2}\right)\left(4\frac{A^2}{d^2}-m^2\right)}\sin\frac{m\pi d}{A} \qquad (A60)$$

APPENDIX B

Detailed Analysis of Lossy Discontinuity

If the discontinuity is not lossless but symmetrical, the Z-parameters of the equivalent circuit will contain both resistive and reactive terms, as shown in Figure B1. As has been noted in section 7.1, we can represent the even input impedance $Z_{ie} = Z_{11} + Z_{12}$ and odd input impedance $Z_{io} = Z_{11} - Z_{12}$ as shown in Figures B2 and B3 respectively.

$Z_{11}+Z_{12}$ can be represented by a section of transmission line of length ℓ_e, being terminated by a pure resistance $R(R > Z_o$, because of voltage maximum at $z = o)$ such that

$$Z_{11}+Z_{12} = \frac{\frac{R}{Z_o} + j \tan k\ell_e}{1+j\frac{R}{Z_o}\tan k\ell_e} \qquad (B1)$$

Similarly $Z_{11} - Z_{12}$ can be represented by a section of transmission line, of length ℓ_o, being terminated by a pure resistance $r(r < Z_o$, because of voltage minimum at $z = o)$ such that

$$Z_{11}-Z_{12} = \frac{\frac{r}{z_o} + j \tan k\ell_o}{1+j\frac{r}{z_o}\tan k\ell_o} \qquad (B2)$$

ℓ_e and ℓ_o can be found directly from the change of resonant wavelength of the ring as follows

$$\ell_e = \frac{1}{2}(n\lambda_{te} - \ell_{ring}) \qquad (B3)$$

$$\ell_o = \frac{1}{2}(n\lambda_{to} - \ell_{ring}) \qquad (B4)$$

The values of R and r can be determined from changes in the resonant Q of the ring. R and r include ohmic and radiation losses due

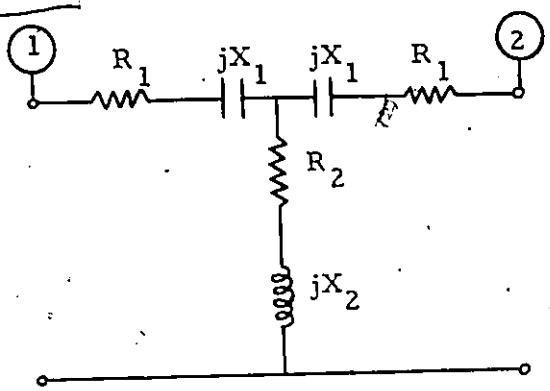

Figure B1 Equivalent circuit for a lossy symmetrical discontinuity

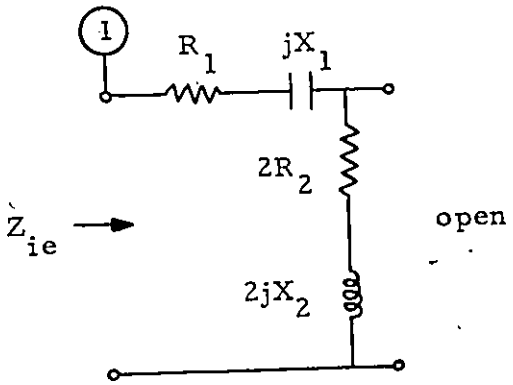

Figure B2 One half of the equivalent circuit for even excitation of lossy symmetrical discontinuity.

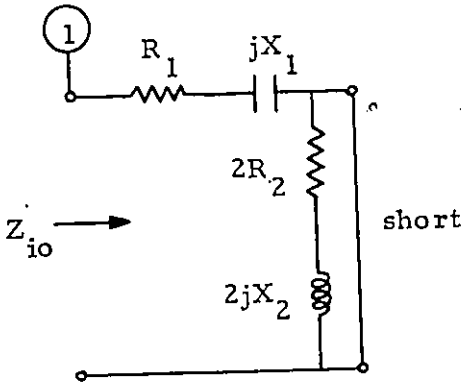

Figure B3 One half of the equivalen circuit for odd excitatio of lossy symmetrical discontinuity.

to the discontinuity.

From the definition of Q factor,

$$Q = \frac{2\pi \times \text{energy stored in the system}}{\text{energy dissipated per cycle in the system}} \quad \text{(B5)}$$

$$Q_{external} = \frac{2\pi \times \text{energy stored in the system}}{\text{energy dissipated per cycle in resistance R or r}} \quad \text{(B6)}$$

a) Even case

During even excitation, let U represent the maximum voltage on the line. So the r.m.s value of the voltage is $U/\sqrt{2}$. Hence the stored energy in the system is given by

$$W_{stored} = \frac{1}{2} C. \frac{U^2}{2} \quad \text{(B7)}$$

where C is the total capacitance of the ring.

Since there are terminations to the fictitious transmission lines by resistances R at both planes 1 and 2, energy dissipated in the resistances per cycle will be given by,

$$W_{dissipated/\,cycle} = 2. \frac{U^2}{2} \cdot \frac{1}{R} \cdot \frac{1}{f} = \frac{U^2}{R.f} \quad \text{(B8)}$$

where f is the frequency of resonance.

Hence, using the expression (B6),

$$Q_{external} = \frac{2\pi \cdot \frac{1}{4} CU^2}{U^2/R.f} \quad \text{(B9)}$$

$$= \frac{\pi}{2} C R f \quad \text{(B10)}$$

Now $C = C' (\ell_{ring} + 2\ell_e)$, where C' = capacitance per unit length of the ring (B11)

and $\ell_{ring} + 2\ell_e$ = extended length of the ring under even excitation

and $$C' = \frac{1}{Z_o f \lambda_t} \quad \text{(B12)}$$

Hence, we can write

$$Q_{external} = \frac{\pi}{2} \cdot \frac{1}{Z_o f \lambda_t} \cdot (\ell_{ring} + 2\ell_e) R f \qquad (B13)$$

$$= \frac{\pi n}{2} \cdot \frac{R}{Z_o} \quad , \text{ since } \lambda_t = \frac{\ell_{ring} + 2\ell_e}{n} \qquad (B14)$$

where n is the harmonic number

Now, if Q_1 is the unloaded Q of the ring and Q_{2e} is the loaded Q of the ring, we can write

$$\frac{1}{Q_{2e}} = \frac{1}{Q_1} + \frac{1}{Q_{external}} \qquad (B15)$$

$$\text{or, } Q_{external} = \frac{Q_1 \, Q_{2e}}{Q_1 - Q_{2e}} \qquad (B16)$$

So, using (B14) and (B16)

$$\gamma \frac{R}{Z_o} = \frac{2}{\pi n} \cdot \frac{Q_1 \, Q_{2e}}{Q_1 - Q_{2e}} \qquad (B17)$$

b) Odd case.

For odd excitation, let I represent the maximum current on the line. So, the r.m.s. value of the current is $I/\sqrt{2}$. Hence the stored energy in the system is given by

$$W_{stored} = \frac{1}{2} L \cdot \frac{I^2}{2} \qquad (B18)$$

where L is the total inductance of the line.

Since resistances r terminate fictitious transmission lines at both the planes 1 and 2, energy dissipated in the resistances per cycle will be given by

$$W_{dissipated}/\text{cycle} = 2 \cdot \frac{I^2}{2} \cdot r \cdot \frac{1}{f} = \frac{I^2 r}{f} \qquad (B19)$$

where f is the frequency of resonance.

Hence using expression (B6),

$$Q_{external} = \frac{2\pi \cdot \frac{1}{4} L I^2}{\frac{I^2 \cdot r}{f}} \qquad (B20)$$

$$= \frac{\pi}{2} \frac{L}{r} \cdot f \qquad (B21)$$

Now, with C as the total capacitance of the ring and C' as the capacitance per unit length of the ring, we can write

$$Q_{external} = \frac{\pi}{2} \cdot \frac{L}{C} \cdot C' (\ell_{ring} + 2\ell_o) \frac{1}{r} \cdot f \qquad (B22)$$

where $(\ell_{ring} + 2\ell_o)$ is the extended length of the ring under odd excitation.

Again, $L/C = Z_o^2$ where Z_o is the characteristic impedance of the line. (B23)

So, $$Q_{external} = \frac{\pi}{2} \cdot Z_o^2 \cdot \frac{1}{Z_o f \lambda_t} (\ell_{ring} + 2\ell_o) \cdot \frac{1}{r} \cdot f \qquad (B24)$$

$$= \frac{\pi n}{2} \cdot \frac{Z_o}{r}, \text{ since } \lambda_t = \frac{\ell_{ring} + 2\ell_o}{n} \qquad (B25)$$

where n is the harmonic number

Now, if Q_1 is the unloaded Q of the ring and Q_{2o} is the loaded Q of the ring, we can write

$$\frac{1}{Q_{2o}} = \frac{1}{Q_1} + \frac{1}{Q_{external}} \qquad (B26)$$

or $$Q_{external} = \frac{Q_1 \, Q_{2o}}{Q_1 - Q_{2o}} \qquad (B27)$$

Hence, using (B25) and (B27)

$$\frac{r}{Z_o} = \frac{\pi n}{2} \frac{Q_1 - Q_{2o}}{Q_1 \, Q_{2o}} \qquad (B28)$$

APPENDIX C

Elimination of the Effect of Capacitive Launcher on the Frequency Measurements

The capacitive launcher is used to launch the wave into the ring resonator. But over and above launching the wave, the launcher adds capacitance to the ring. Hence the length of the ring resonator is effectively greater than the measured physical mean length by an amount that represents the above mentioned capacitive effect. An increased length of the ring, in turn, means the measured resonant frequencies will be lower than the correct ones. By correct values of resonance frequencies here we mean the measurements that would have been possible if the effect of the capacitive launcher were not present. We shall describe a way to find the correct values of the resonant frequencies from the measured ones.

It is evident that the smaller the gap between the launcher and the ring, the higher is the value of the capacitance. Consequently the measured frequency deviates further from the correct value. If the gap width is increased, the effect of the capacitance is decreased and consequently the measured frequency approaches the correct value. This fact that the measured frequencies approach the correct value forms the basis of the method of elimination of capacitance we are describing here.

Let us take a frequency measurement with gap width d very small. Then by increasing d in a few steps, the corresponding values of frequency are measured. The 1/d versus frequency plot will now give the way the changes are occurring, as shown by the solid line in Figure C1. If we now extrapolate the curve, the point where it intersects the frequency axis shall give us the frequency for infinite gap width. This is the correct value of the frequency that we wanted because, infinite gap width though not practially possible, means the launcher is absent.

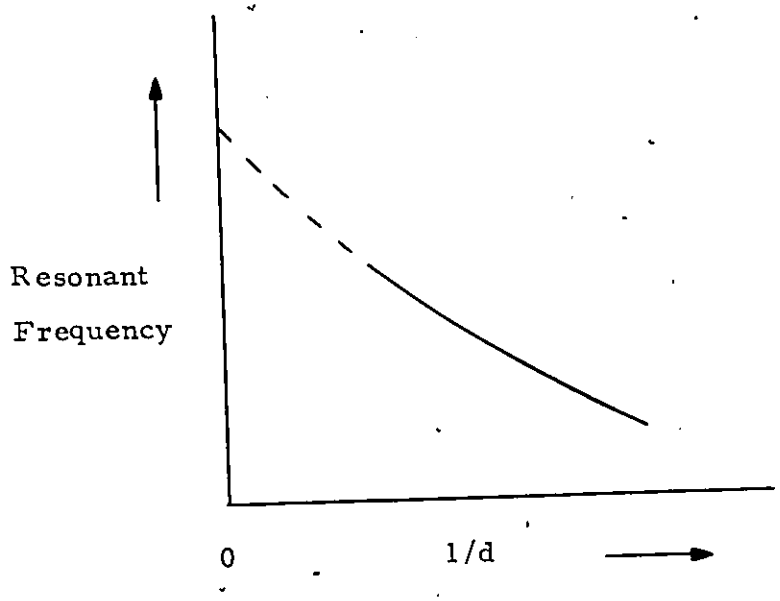

Figure C1 Inverse of launcher-gap-width versus resonant frequency plot.

As an example of this method, we have studied the resonance frequencies of the empty ring resonator of length $\ell_{ring} = 57.375$ cm for different launcher gap width. The results are shown in Table C1. For each harmonic number one graph was plotted and the extrapolated value of the frequency for infinite gap width was obtained.

Table C 1

Dependence of Resonant Frequencies on Launcher Gap Width

(Empty Stycast line, ε_r = 10.6, w/h= 2.7, h= 5 mm, Z_0= 27 ohms, ℓ_{ring} =57.375 cm)

Gap Width d (mm)		0.187	0.460	0.887	∞ (projected)
1/d		5.342	2.174	1.127	0
Resonance Frequency (MHz) for harmonic number n =	1	193.331	193.370	193.445	193.543
	2	386.523	386.640	386.747	386.900
	3	575.756	575.875	576.082	576.270
	4	762.799	762.953	763.190	763.500
	5	947.170	947.173	947.613	948.090
	6	1129.500	1129.674	1130.015	1130.450
	7	1309.884	1310.081	1310.387	1310.980
	8	1488.480	1488.612	1489.017	1489.780
	9	1664.636	1664.996	1665.308	1665.730
	10	1839.920	1840.116	1840.604	1841.320

APPENDIX D

Radiation from Thin Transverse Discontinuity in a Microstrip

L. Lewin [24] has developed a method of calculation of radiation from discontinuities in a microstrip transmission line. In our present work we have considered the cases of thin transverse metallic obstacles and circular cylindrical metallic posts. To have an idea of the amount of power that is radiated (compared to the incident power) from these types of discontinuities, we shall present here Lewin's expression for thin transverse obstacles. We shall also present the numerical values, calculated on the basis of the above mentioned expression, of radiated power (as a fraction of incident power) from two thin transverse metallic obstacles which we have actually studied in our laboratory experiments.

Accordin to Lewin, the ratio of the radiated power to the power incident on a thin transverse reactive obstacle in a microstrip transmission line is given by

$$P_R = 60 \frac{(kh)^2}{Z_o} \cdot \frac{1}{1+4X^2} \cdot \left[3 - \frac{1}{\varepsilon_{eff}} - \left(3 + \frac{1}{\varepsilon_{eff}}\right) \frac{\varepsilon_{eff}-1}{2\sqrt{\varepsilon_{eff}}} \ln \frac{\sqrt{\varepsilon_{eff}}+1}{\sqrt{\varepsilon_{eff}}-1}\right] \quad (D1)$$

where $k = \frac{2\pi}{\lambda}$ [λ is the free space wavelength]

h = dielectric thickness

Z_o = characteristic impedance of the microstrip line

X = normalized reactance of the transverse obstacle

ε_{eff} = effective dielectric constant

In the laboratory experiments we have studied two thin transverse metallic obstacles of width d = 1.62 mm and d = 3.07 mm. For these obstacles, we have determined the different even resonance frequencies

and the coresponding values of ε_{eff} and normalized reactance (see Tables 9.3, 9.4, 9.5, 9.6). Using these data and equation (D1), we have calculated the values of P_R. These are presented in Tables D1 and D2 and Figure D1. These values of P_R clearly show that, for transverse reactive obstacles in microstrip line, a very tiny fraction of the incident power is radiated.

Table D 1

Ratio of Radiated Power to Incident Power (for Thin Transverse Reactive Obstacles) at different frequencies

(Stycast line, ε_r= 10.6, w/h= 2.7, h= 5 mm, Z_0= 27 ohms, Obstacle Width d= 1.62 mm)

Frequency (MHz)	Radiated Power / Incident Power
272.205	0.34674×10^{-4}
453.867	0.83228×10^{-4}
634.692	1.36385×10^{-4}
815.236	1.89562×10^{-4}
994.279	2.36558×10^{-4}
1172.034	2.76991×10^{-4}
1348.419	3.08294×10^{-4}
1523.640	3.34524×10^{-4}
1697.852	3.67800×10^{-4}
1870.088	3.71583×10^{-4}

Table D 2

Ratio of Radiated Power to Incident Power (for Thin Transverse Reactive Obstacles) at different frequencies

(Stycast line, ε_r= 10.6, w/h = 2.7, h= 5 mm, Z_0= 27 ohms, Obstacle Width d= 3.07 mm)

Frequency (MHz)	Radiated Power / Incident Power
276.285	0.36995×10^{-4}
459.256	0.92157×10^{-4}
641.508	1.59335×10^{-4}
821.963	2.27637×10^{-4}
1001.990	3.01015×10^{-4}
1180.038	3.68089×10^{-4}
1355.664	4.13938×10^{-4}
1531.384	4.74034×10^{-4}
1705.924	5.41924×10^{-4}
1876.676	5.33705×10^{-4}

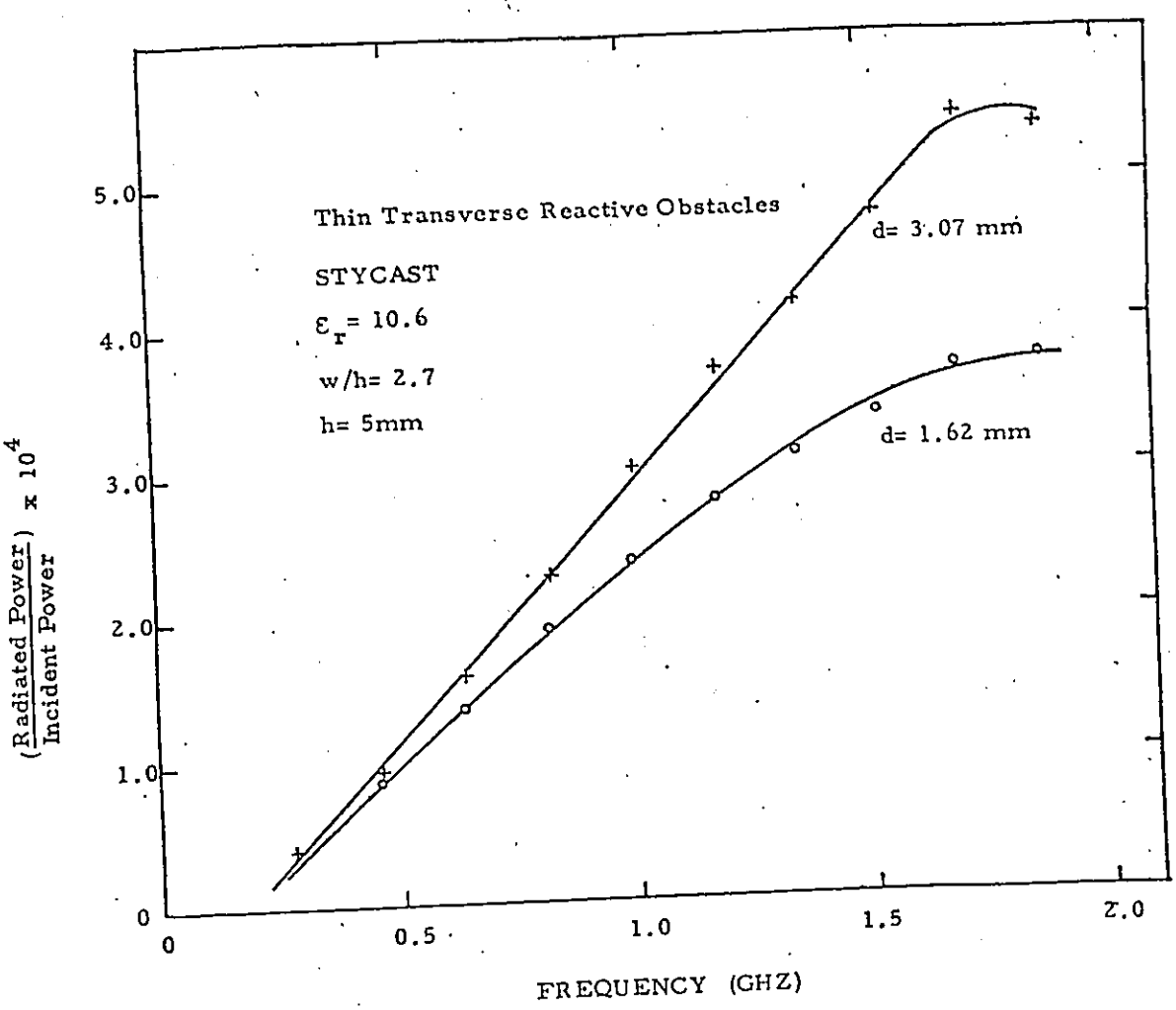

Figure D1 Ratio of Radiated power to Incident power for thin transverse reactive obstacles. Obstacle width d= 1.62mm , d= 3.07mm

APPENDIX E

A note on the use of Wheeler's parallel plate model by Wolff, Kompa and Mehran [26]

Wheeler's parallel plate model was used by Wolff, Kompa and Mehran [26] to find the scattering matrix of two types of microstrip discontinuity, namely an abrupt change of width of the line and the T-junction. They used mode matching technique for fields on both sides of the discontinuity. Disagreement between their theory and the measurements was quite considerable. So, they had to introduce some correction terms to account for radiation. This is not surprising because the discontinuities investigated by these authors are mainly situated at the extremities of the microstrip cross-section where the model differs very strongly from the original line. It appears that the closer the discontinuity is situated to the center of the microstrip cross-section, the better are the results obtained by the parallel plate model.

REFERENCES

1. A. Farrar and A. T. Adams,'' Matrix Methods for Microstrip Three-Dimensional Problems,'' IEEE Trans. on Microwave Theory and Techniques, vol. MTT-20, No. 8, August 1972, pp. 497-504.
2. P. Benedek and P. Silvester,'' Equivalent Capacitances for Microstrip Gaps and Steps,'' IEEE Trans. on Microwave Theory and Techniques, vol. MTT-20, No. 11, November 1972, pp. 729-733.
3. P. Silvester and P. Benedek,'' Equivalent Capacitances of Microstrip Open Circuits,'' IEEE Trans. on Microwave Theory and Techniques, vol. MTT-20, No. 8, August 1972, pp. 511-516.
4. M.Maeda,'' An Analysis of Gap in Microstrip Transmission Lines,'' IEEE Trans. on Microwave Theory and Techniques, vol. MTT-20, No. 6, June 1972, pp 390-396.
5. P. Silvester and P. Benedek,'' Microstrip Discontinuity Capacitances for Right-Angle Bends, T Junctions and Crossings,'' IEEE Trans. on Microwave Theory and Techniques, vol. MTT-21, No. 5, May 1973, pp. 341-346.
6. R. Horton,'' The Electrical Characterization of a Right-Angled Bend in Microstrip Line,'' IEEE Trans. on Microwave Theory and Techniques, vol. MTT-21, No. 6, June 1973, pp. 427-429.
7. A. Gopinath and B. Easter,'' Moment Method of Calculating Discontinuity Inductance of Microstrip Right-Angled Bends,'' IEEE Trans. on Microwave Theory and Techniques, vol. MTT-22, No. 10, October 1974, pp. 880-883.
8. H. A. Wheeler,'' Transmission-Line Properties of Parallel Strips Separated by a Dielectric Sheet,'' IEEE Trans. on Microwave Theory and Techniques, vol. MTT-13, No. 3, March 1965, pp. 172-185.
9. M. A. R. Gunston and J. R. Weale,'' The Transmission Characteristics of Microstrip,'' The Marconi Review, Third Quarter, 1969, pp. 226-243.

10. I. M. Stephenson and B. Easter,'' Resonant techniques for establishing the equivalent circuits of small discontinuities in microstrip,'' Electronics Letters, vol. 7, No. 19, 1971, pp. 582-584.

11. R. J. P. Douville and D. S. James,'' Experimental characterization of microstrip bends and their frequency dependent behaviour,'' IEEE Int. Electrical, Electronics Conference and Exposition, Toronto, Ontario, Canada, 1973.

12. H. Groll and W. Weidmann,'' Measurement of equivalent circuit elements of microstrip discontinuities by a resonant method,'' Nachrichtentech, Z., vol. 28, January 1975, pp. 74-77.

13. N. Marcuvitz, Waveguide Handbook, Boston, Mass.: Boston Tech.,1964.

14. W. J. R. Hoefer and G. R. Painchaud,'' Frequency markers providing resolution of 1KHz for swept microwave measurements,'' Electronics Letters, vol. 10, April 1974, pp. 123-124.

15. W. J. R. Hoefer and A. Chattopadhyay,'' Measurement of the equivalent circuit parameters of discontinuities in a resonant microstrip ring,'' 1975 Int. Microwave Symposium, Palo Alto, California.

16. W. J. R. Hoefer and A. Chattopadhyay,'' Evaluation of the Equivalent Circuit Parameters of Microstrip Discontinuities through Perturbation of a Resonant Ring,'' IEEE Trans. on Microwave Theory and Techniques, vol. MTT-23,No. 12, December 1975, pp. 1067-1071.

17. A. Chattopadhyay and W. J. R. Hoefer,'' Error Analysis for Characterization of Microstrip Discontinuities in Resonant Rings,'' IEEE Int.Electrical, Electronics Conference and Exposition, Toronto, Ontario,Canada, 1975.

18. A. Chattopadhyay and W. J. R. Hoefer,'' General Analysis of Measurement of Microstrip Discontinuity Parameters in a Resonant Ring,'' the University of Ottawa, Dept. of Electrical Engineering Technical Report No. TR-76-1, January 1976.

19. W. J. R. Hoefer,'' Computerized Evaluation of Scattering on Thin Transverse Obstacles in Microstrip,'' Fourth ICEE Conference, Shiraz, Iran,1974.

20. W. J. R. Hoefer and D. S. James, "A variational expression for the reactance of transverse microstrip discontinuities," 1974 IEEE Canadian Conf. on Communication and Power, Montreal, Canada.

21. J. Schwinger and D. S. Saxon, Discontinuities in Waveguides, Gordon and Breach Science Publishers, New York, 1968, pp. 12-48.

22. J. A. Stratton, Electromagnetic Theory, McGraw Hill, 1941, pp. 372-374.

23. P. Troughton, "Measurement techniques in microstrip," Electronics Letters, vol. 5, No. 2, January 1969, pp. 25-26.

24. L. Lewin, "Radiation from Discontinuities in Strip-line," Proc. of IEE, February 1960, pp. 163-170.

25. W. Groebner and N. Hofreiter, Integraltafel - Zweiter Teil: Bestimmte Integrate, Springer Verlag, Wien und Innsbruck, 1950.

26. I. Wolff, G. Kompa and R. Mehran, "Calculation method for microstrip discontinuities and T-junctions," Electronics Letters, vol. 8, No. 7, April 1972, pp. 177-179.

27. O.P. Jain, "A Study of Dispersive Behaviour in Microstrip Transmission Lines," Carleton University, Faculty of Engineering, Technical Report, May 1971.

V I T A

Name : Asoknath Chattopadhyay

Born : Jamshedpur, India ; February 10, 1947

Education :

Secondary : Serampore Union Institution, West Bengal, India

University : St. Xavier's College,
University of Calcutta.
B. Sc. with Honors in Physics, 1965

Institute of Radio Physics and Electronics,
University of Calcutta.
B. Tech., 1967
M. Tech., 1968

Department of Electrical Engineering,
University of Ottawa.
M. A. Sc., 1971